# Modeling ice algae in the Canadian Arctic Archipelago

by Lynn Pogson

Department of Atmospheric and Oceanic Sciences

McGill University, Montreal

July 2009

A thesis submitted to McGill University in partial fulfilment of the requirements of the degree of Master of Science

©Lynn Pogson, 2009

## Acknowledgements

This thesis would not have been possible without my supervisor Bruno Tremblay, who sparked my interest in this subject and provided guidance and advice along the way. I am also very grateful to Diane Lavoie, Christine Michel, and Martin Vancoppenolle for sharing code and data, as well as engaging in discussions on numerous topics to help in my understanding. I would also like to thank my parents, for their comments and suggestions during the editing process. Finally, a thanks to Eyad Atallah for providing me with Environment Canada data, and to David Huard for translating my abstract to french.

## Contents

| $\mathbf{A}$ | bstra | $\operatorname{ct}$ |                             | vi |
|--------------|-------|---------------------|-----------------------------|----|
| 1            | Intr  | oducti              | ion                         | 1  |
|              | 1.1   | Motiva              | ation                       | 1  |
|              | 1.2   | Object              | tives                       | 3  |
|              | 1.3   | Litera              | ture Review                 | 4  |
|              |       | 1.3.1               | Carbon fluxes               | 4  |
|              |       | 1.3.2               | Ice algae importance        | 6  |
|              |       | 1.3.3               | Growth factors              | 7  |
|              |       | 1.3.4               | Hospitable ice conditions   | 10 |
|              |       | 1.3.5               | Bloom dynamics              | 13 |
|              |       | 1.3.6               | Ice algae modeling          | 14 |
| 2            | Mo    | del des             | scription                   | 17 |
|              | 2.1   | Therm               | nodynamic snow ice model    | 17 |
|              |       | 2.1.1               | Algae thermodynamic effects | 21 |
|              | 2.2   | Ice alg             | gae - nutrient model        | 23 |
|              |       | 2.2.1               | Governing equations         | 23 |
|              |       | 2.2.2               | Platelet layer              | 24 |
|              | 2.3   | Coord               | inate Transformation        | 27 |
|              |       | 2.3.1               | Thermodynamic model         | 27 |
|              |       | 2.3.2               | Algae-nutrient model        | 29 |

|   |     | 2.3.3   | Internal algae advection   | . 30 |
|---|-----|---------|----------------------------|------|
|   |     | 2.3.4   | Advection at the ice base  | . 31 |
|   | 2.4 | Numer   | rical scheme               | . 33 |
|   |     | 2.4.1   | Internal layers            | . 34 |
|   |     | 2.4.2   | Bottom ice layer           | . 37 |
|   |     | 2.4.3   | Ice base                   | . 38 |
| 3 | Dat | a       |                            | 39   |
| 4 | Res | ults ar | nd Discussion              | 41   |
|   | 4.1 | Ice/sn  | ow thickness comparison    | . 42 |
|   | 4.2 | PAR a   | at the ice base            | . 42 |
|   | 4.3 | Algal   | bloom                      | . 45 |
|   | 4.4 | Sensiti | ivity Analysis             | . 51 |
|   |     | 4.4.1   | Brine flushing             | . 51 |
|   |     | 4.4.2   | Freshwater lens            | . 52 |
|   |     | 4.4.3   | Self shading               | . 53 |
|   |     | 4.4.4   | Oceanic heat flux          | . 56 |
|   |     | 4.4.5   | Viscous sublayer thickness | . 58 |
|   |     | 4.4.6   | Grazing                    | . 60 |
|   |     | 4.4.7   | Biomass initial condition  | 61   |
| 5 | Con | clusio  | n                          | 63   |
|   |     |         |                            |      |

| 6                | Ref  | erences  | 66         |
|------------------|------|--|------------|
| $\mathbf{A}_{]}$ | ppen | dices  | 73         |
| A                | Inte | ernal melting  | 73         |
| В                | Mo   | del Validation   | <b>7</b> 5 |
|                  | B.1  | Nutrients and algae advection                            | 75         |
|                  | B.2  | Algae/nutrient loss at ice base                          | 78         |
|                  | В.3  | Nutrient influx at the ice base                          | 80         |
|                  | B.4  | Nutrient uptake  | 80         |
| ${f L}$          | ist  | of Figures   |            |
|                  | 1    | Sea ice model schematic                                  | 19         |
|                  | 2    | Under-ice nutrient schematic                             | 25         |
|                  | 3    | Coordinate transformation of the snow and ice components | 27         |
|                  | 4    | Location of study site                                   | 39         |
|                  | 5    | Simulated ice thickness versus observations              | 43         |
|                  | 6    | PAR site results   | 46         |
|                  | 7    | HSC and LSC site results                                 | 49         |
|                  | 8    | Simulated biomass growth and loss                        | 50         |
|                  | 9    | Simulated and observed silicic acid concentrations       | 50         |
|                  | 10   | Simulated biomass with new flushing term                 | 52         |

| 11   | Simulated biomass with melt lens                               | 54 |
|------|--|----|
| 12   | Simulated biomass through different ice layers                 | 55 |
| 13   | Oceanic heat fluxes comparison                                 | 57 |
| 14   | Biomiass sensitivity to the oceanic heat flux                  | 59 |
| 15   | Biomass sensitivity to the viscous sublayer thickness          | 60 |
| 16   | Biomass sensitivity to grazing                                 | 61 |
| 17   | Biomass sensitivity to initial condition                       | 62 |
| 18   | Advection term validation                                      | 77 |
| 19   | Validation of loss term at ice base                            | 79 |
| 20   | Nutrient influx validation                                     | 81 |
| 21   | Nutrient uptake validation                                     | 83 |
| List | of Tables  |    |
| 1    | Some physical parameters and constants in the snow ice model . | 21 |
| 2    | Photosynthetic parameters for the 3 data sites                 | 41 |

#### Abstract

Ice algae are an important component of the carbon cycle in the Arctic, and can therefore have an impact on climate. I investigate the dynamics of an ice algae bloom by coupling an algae-nutrient model [Lavoie et al., 2005] with a thermodynamic sea ice model [Huwald et al., 2005]. The sea ice component is a more sophisticated model than what has been used in past Arctic ice algae model studies. To validate the model, I simulate an algal bloom at the base of the ice over a season and compare with data from the Resolute area in the Canadian Arctic Archipelago. Results suggest that bloom dynamics are strongly related to the ice growth/melt rate, with ice melt being the trigger for bloom decline. Being able to accurately model physical conditions is essential before ice algae can be accurately modeled, and some recommendations for improvement are discussed.

Les algues de glace sont une composante importante du cycle du carbone dans l'Arctique et peuvent avoir une influence sur le climat. J'explore la dynamique d'une efflorescence algale par le couplage d'un modèle d'algues /nutriments [Lavoie et al., 2005] avec un modèle de la thermodynamique de la glace de mer [Huwald et al., 2005]. Le modèle de glace est plus sophistiqué que les modèles utilisés dans les études précédentes sur les algues de glace Arctiques. Pour valider le modèle, je simule une efflorescence algale à la base de la glace pendant une saison et on compare avec des données de la région de Resolute dans l'Archipel Canadien Arctique. Les résultats indiquent que la dynamique de l'efflorescence est fortement liée au taux de croissance et de fonte, la fonte étant le déclencheur du déclin de l'efflorescence. La capacité de modéliser avec précision les conditions physiques est essentiel pour simuler correctement les algues de glaces, et quelques améliorations sont suggérées.

## 1 Introduction

#### 1.1 Motivation

The Arctic is a region of particular interest to climate scientists, with general circulation models all suggesting that the Arctic Ocean and its surrounding seas will undergo a more intense increase in temperature than anywhere else [Johannessen et al., 2004]. An important question to answer in the context of climate change is: how will warming affect the flux of carbon through the Arctic? With a diminishing ice cover, increasing river runoff and more permafrost thawing, a warming Arctic will likely bring with it more production of CO<sub>2</sub> through bacterial activity and photooxidation in surface waters [Belanger et al., 2006]. On the other hand, changing Arctic conditions may provide more nutrient and light availability for autotrophs to perform photosynthesis and sequester carbon [Gobeil et al., 2001]. The flux of carbon through the system and the contribution of each of the above mentioned processes must be explained in the quest to understand climate change effects in the Arctic.

This thesis focuses on ice algae, which contribute to primary production, provide food to the pelagic food web, and play an important role in drawdown of CO<sub>2</sub> to the sea floor. Ice algae rely on the presence of an ice cover, and changing conditions will have varying effects. While increased availability of nutrients and light would likely increase the growth of ice algae in a warming Arctic, higher temperatures and earlier snow melts could result in a higher loss of algae from melt at the ice base and reduction of nutrient supply [Lavoie et al., 2005]. Developing an ice algae model can help predict how algal blooms will change in different Arctic environments.

As well as predicting how algae react to a changing Arctic, models can also

provide insight where observations cannot. Data relevant to studying ice algae dynamics in the Arctic is limited or non-existent because of the difficulty of accessing the area and the severe environmental conditions [Lavoie et al., 2008]. For these reasons, most studies are conducted in spring or summer, at a time when ships can navigate the area more easily [Lavoie et al., 2008]. As a result, there are significant spatial and temporal gaps, impeding the understanding of why and how algal blooms develop. By filling in the gaps in data, numerical models can do a better job in explaining the dynamics of ice algae and the role various factors may play in controlling algal blooms.

Modeling studies in the Arctic in the past have focused on algal blooms at the base of the ice, in the first 1 to 4 cm of Arctic first year ice where ice algae are overwhelmingly located [Smith et al., 1988]. However algal communities have been observed to develop at all levels (surface, freeboard, interior and bottom) of the ice column [Cota and Smith, 1991]. Indeed, a study by Gradinger [1999] of the biomass and composition of algal communities in multi-year ice in the central Arctic during two summers revealed high biomass accumulations at the surface and in the interior as well as in the bottom layer of ice. In addition, it was found that the bottom 20 to 40 cm of ice contained between 4% and 62% of the total algal biomass [Gradinger, 1999]. A large contrast between this study and those from coastal locations indicates that there are different biological regimes in Arctic ice, and suggests that to successfully model ice algae, more than just the community at the ice base needs to be considered [Gradinger and Zhang, 1997].

## 1.2 Objectives

The goal of this project is to develop a snow-ice-algae-nutrient column model to help describe and understand the dynamics of ice algae in Arctic first year and multi-year ice. This thesis presents a snow-ice-algae model with a more complex and physically based snow-ice component than in past models of the Arctic. The algae-nutrient component is based on that of *Lavoie et al.* [2005], while the snow-ice component is that of *Huwald et al.* [2005]. The objective of this work is to couple the algae and snow-ice models and to compare the results with observations to ensure that this new model can accurately simulate Arctic spring algal blooms at the base of first year ice.

#### 1.3 Literature Review

#### 1.3.1 Carbon fluxes

To understand climate change in the Arctic, it is important to determine how the flux of carbon will evolve, and how the  $CO_2$  sources and sinks will balance.

Photochemical oxidation of dissolved organic carbon (DOC) in Arctic waters is a source of CO<sub>2</sub>. Given that the ultraviolet (UV) radiation reaching surface waters depends on the sea ice cover and thickness, it is significant to note that observations over the last 3 decades have shown a 20% decrease in the spatial extent of sea ice cover and areas of thinning ice in several regions of the Arctic Ocean [Cavalieri et al., 2006]. With summer ice cover expected to continue to decline and completely disappear by the end of the century, UV radiation reaching the water column is expected to increase [Belanger et al., 2006]. Adding to this effect is the recent report of increased UVB (280-320 nm) radiation at the sea surface in northern latitudes, due to a decrease in stratospheric ozone concentration [Fioletov et al., 2004]. Thus with higher levels of UV radiation and ice extent continuing to decline, it is expected that the amount of photochemically active UV radiation (280-400 nm) reaching the surface of Arctic waters will accelerate in the coming decades [Belanger et al., 2006].

The amount of UV radiation for photooxidation is not the only factor to consider. Through river runoff, organic carbon available for photooxidation is expected to increase with changing climate conditions as well [Arnell, 2005]. The Arctic Ocean constitutes 1% of the volume of the world's oceans but currently receives 10% of the freshwater input, making it strongly influenced by this input [Aagaard and Carmack, 1989]. The amount of freshwater and

organic carbon going into the Arctic Ocean will likely increase substantially over this century, by as much as 24% to 31% by 2080 [Arnell, 2005]. In addition to river runoff, the thawing of permafrost is expected to increase the terrestrial organic carbon reaching the Arctic Ocean [Belanger et al., 2006]. A gradual thaw of permafrost has been observed since the 1960s, and part of the sequestered carbon that has been mobilized could be transferred to the ocean by streams and rivers [Benner et al., 2004]. Additionally, a key contribution to the export of organic terrestrial carbon to the ocean is through more coastal erosion, amplified by stronger waves [Grigoriev et al., 2004]. Thus in a warming Arctic, it is expected that the input of organic carbon into the ocean will increase, and there will be more UV radiation penetrating surface waters. Both of these changes are expected to lead to more production of CO<sub>2</sub> through photooxidation.

Another contribution to greenhouse gas production in the Arctic is through bacterial activity. Part of the carbon mobilized during permafrost thawing is oxidized by bacterial action, a major source of CO<sub>2</sub> and methane [Liebner and Wagner, 2006]. Since methane has a greenhouse effect that is as much as 63 times more effective per molecule than that of CO<sub>2</sub>, as the climate warms the Arctic could become a large source of greenhouse gas production [Christensen and Cox, 1995].

However, with a thinner and less extensive ice cover, more shortwave radiation can reach basal ice and the upper ocean mixed layer, where autotrophs undertake photosynthesis. Furthermore, the increased river runoff is expected to bring to the ocean more nutrients from the land, a necessary ingredient for autotrophs to grow [Gobeil et al., 2001]. These nutrients could also become more available because of increased wind mixing and upwelling [Carmack et al.,

2004]. The resulting increase in primary production could play an important role as a CO<sub>2</sub> sink [Gobeil et al., 2001] and perhaps balance the CO<sub>2</sub> produced through photooxidation and bacterial activity. Which of these processes will dominate is a key question for climate scientists to answer.

#### 1.3.2 Ice algae importance

In both the Antarctic and the Arctic, ice algae account for a sizable portion of primary production, one study estimating that at least 25% of the annual production in seasonally ice-covered areas of the Arctic is associated with ice algae [Legendre et al., 1992]. Ice algae are also a source of food for a variety of animals either living on the underside of the sea ice or in the basal ice [Gradinger, 1996]. Using a mass balance argument, Michel et al. [1996] showed that a large portion of the algal biomass expelled into the upper water column during the melt season stayed suspended and was consumed by under-ice grazers. This suggests that ice algae are a food source not only during the height of production within the ice but also during ice melt. If algae shed from ice do not sink and are not ingested by grazers, they can act as a seed for open-water phytoplankton blooms [Michel et al., 1996]. In this way the ice algae (consisting mostly of pennate diatoms) have an influence on the structure of the pelagic food web [Leventer, 2003].

Besides the important role they play in the polar ecosystem, ice algae also contributes to  $CO_2$  drawdown into the deeper areas of the Arctic Ocean [Lavoie et al., 2005]. The speed at which the algae are ejected during ice melt and their physiological condition determine whether they will remain suspended in the surface layer or sink to greater depths [Lavoie et al., 2008]. The amount

of carbon exported to the deep ocean is greater if fast-sinking aggregates are formed [Michel et al., 1996]. While phytoplankton form fast-sinking and slow-sinking aggregates, ice algae only form fast-sinking aggregates [Riebesell et al., 1991]. In addition, ice algae are more "sticky", which means they tend to form aggregates that can sink more rapidly [Riebesell et al., 1991]. Thus, overall, ice algae contribute more to the detrital pool than to total primary production, and play an important role in carbon export [Lavoie et al., 2008].

#### 1.3.3 Growth factors

How these algal blooms in the Arctic develop is in large part determined by the unique environmental conditions in the region. With a permanent ice cover, low water temperature and dark polar winter severely inhibiting biological production, the Arctic has been considered to be one of the most oligotrophic of the world's oceans [Platt and Subba Rao, 1975]. Before trying to model or predict how ice algae will be influenced by different environmental conditions, it is important to first pinpoint what factors determine the rates of algal production and accumulation [Lavoie et al., 2005]. They can be narrowed down to light, nutrients and substrate, and these 3 factors can explain algae variability in different conditions [Lavoie et al., 2005]. These conditions include changes to nutrient concentration and flux, latitude (shortwave radiation availability), snow cover, temperature, grazers, other loss terms such as respiration and sinking, ice structure, stratification, salinity, and currents [Cota and Smith, 1991. It is occasionally suggested that temperature is one of the factors that limits the rate of growth in the same manner as light or nutrients; however, temperature determines a thermodynamic upper limit for growth in any environment, and thus it could be similarly argued that temperature in some way limits growth in tropical waters as well [Arrigo et al., 1993]. Therefore, generally the main controlling factors are considered to be light and nutrients [Lavoie et al., 2005].

The sources of nutrients for ice algae are through brine drainage, in situ regeneration of biogenic materials, and exchanges with the mixed layer [Meguro et al., 1967. Where the algae are situated in the ice will affect which supply of nutrients is more important; for example the principal supply of nutrients for bottom ice algae is from the water column [Cota and Smith, 1991]. Obtaining direct measurements of nutrient concentrations at the base of the ice is difficult, but determining if algae is nutrient limited can be done indirectly [Lavoie et al., 2005. Nutrient ratios and distributions, changes in biomass, photosynthetic performance, and biochemical composition all may suggest that the algae is nutrient limited [Lavoie et al., 2005]. Since the underlying water column is the main nutrient source for algae at the ice base, it is expected that a steep gradient of nutrients exists from the ice-water interface upwards [Cota and Smith, 1991. Indeed in fine-scale profiles seen in the high Arctic, inorganic nutrients do form such gradients through the basal algal communities observed [Smith et al., 1990. While nitrate and phosphate concentrations are remarkably high in Arctic basal ice and correlate with chlorophyll concentrations, silicate levels in the ice are not significantly higher than in the underlying seawater [Cota et al., 1990]. This observation reflects the ability of algal cells to store excess nitrates and phosphates but not silicates, and it is for this reason that silicic acid is considered the limiting nutrient for algal productivity [Cota and Smith, 1991].

The supply of nutrients to the bottom layer of ice is influenced by several fac-

tors, including ice melt or growth rate. During ice growth the nutrient flux is enhanced by convection at the ice base [Cota et al., 1991], while during ice melt freshwater at the base of the ice increases stratification and lowers the flux of nutrients [Gosselin et al., 1985]. In general, the flow of nutrients from the water column is governed by diffusion across the viscous sublayer below the ice base [Lavoie et al., 2005]. This sublayer thickness can be affected by tidal mixing. Friction velocity changes over the tidal cycle, which alters the thickness of the viscous layer and in turn the nutrient flux [Lavoie et al., 2005]. Observations of nutrient ratios and distributions, changed biomass and other factors suggest that there is a limitation of nutrients for algal growth during neap tide when the viscous layer is thickest [Cota and Horne, 1989].

Irradiance is thought to be the most dominant factor controlling ice algae growth and biomass distribution in space and time [Cota and Smith, 1991]. The amount of light reaching polar waters is extremely variable because of the presence of the ice and snow cover, and algal blooms occur in the spring when enough light becomes available [Gradinger, 1996]. Part of the irradiance reaching the surface of the ice is reflected - more so if a snow cover is present [Smith et al., 1988]. Surface albedo can range from less than 0.3 for ice covered with melt ponds to over 0.8 for snow-covered ice [Gradinger, 1996]. Attenuation within snow and ice further reduces the irradiance reaching the algae concentrated at the ice base [Smith et al., 1988]. Snow cover has the largest effect on light extinction, with an attenuation coefficient ranging from 4.3 m<sup>-1</sup> in dense snow to 40.1 m<sup>-1</sup> in fresh snow, versus about 1.2 m<sup>-1</sup> for ice [Grenfell and Maykut, 1977]. The pattern of algal biomass at the bottom of the ice overall follows the seasonal trend in solar radiation, with the greatest and most rapid accumulation occurring under a thin snow cover with higher light levels [Cota and Smith, 1991]. During the winter, irradiance levels are

extremely low and follow a light-dark cycle [Cota and Smith, 1991]. As irradiance increases through the spring, enough light becomes available to support algal photosynthesis and growth [Fortier et al., 2002], and the start of the bottom algal bloom follows [Michel et al., 1996]. Although irradiance plays a key role in ice algal growth and distribution, other factors have an influence on the accumulation of biomass as well.

#### 1.3.4 Hospitable ice conditions

A study done in a subpolar estuary by Gosselin et al. [1986] concluded that although snow cover thickness, through its influence on irradiance levels in the ice, was the most important factor controlling biomass distribution over tens of metres, it is salinity and its influence on ice structure that are the dominant factors over kilometre scales. Salts are present in pockets of brine in the ice, which enlarge and become interconnected in response to internal stresses and increased temperatures [Vancoppenolle et al., 2007]. This network of partially interconnected brine channels makes up 1% to 30% of the ice volume [Meiners et al., 2003 and enables transport of brine through the ice [Horner et al., 1992. Salinity in the ice changes as brine moves through the ice in processes including brine expulsion, brine drainage, and flushing | Vancoppenolle et al., 2007. These channels generally form in the spring when melting helps to connect multiple channels, opening up flow with the nutrient-rich water column [Weeks and Ackley, 1986]. Thus the presence of brine and its associated dynamics seems to affect not only sea ice thermodynamic properties but the supply of nutrients to the ice algae as well [Vancoppenolle et al., 2007].

The structure of the ice also has a large effect on the vertical distribution of

ice algae [Ackley et al., 1979]. Algae may be scattered between ice crystals with no pattern in their distribution or, more commonly, concentrated in the brine channels [Meiners et al., 2003]. Ice algae attach themselves along the brine channel walls, but there is evidence that they have the ability to maintain their vertical position relative to the platelet ice layer at the bottom of the ice and not become incorporated into the crystal matrix as the ice grows [Welch and Bergmann, 1989]. By moving along as the ice sheet thickens, the ice algae maintain their supply of nutrients and avoid being frozen into the sea ice matrix [Arrigo et al., 1993].

The influence of different ice structures on ice-dwelling organisms is illustrated by comparing Arctic sea ice with Antarctic ice. The age and thickness of the ice in the Arctic are on average greater than in the Antarctic [Spindler, 1990]. While the Antarctic is almost entirely thin first year ice, the majority of Arctic ice is multi-year ice and greater than 2 m thick [Johannessen et al., 2004]. Because of more turbulent waters during formation, it is also common for Antarctic ice to be more granular than Arctic ice, allowing additional room within the ice for organisms [Horner et al., 1992]. Thus the distribution of ice algae in the Arctic is not as vertically extensive as that of ice algae in the Antarctic, which can be found at the snow-ice interface, at the freeboard layer, in the interior of the ice, and in the bottom layer [Gradinger, 1999].

As mentioned, in the coastal Arctic ice an overwhelming amount of algal biomass is concentrated in the bottom few centimetres [Gradinger, 1999]. Coastal ice is defined as ice that forms and remains frozen to the shore, and is where the majority of Arctic ice biological studies have been conducted [Horner et al., 1992]. Pack ice (any area of sea ice not considered coastal ice) is more likely to feature internal communities of ice algae which, with the exception

of coastal areas with multi-year ice, are rarely present in coastal ice [Arrigo et al., 1993]. The majority of pack ice is multi-year ice which, having undergone a spring melt, has a more porous interior for algae to grow [Meiners et al., 2003]. Spring blooms of ice algae are common in coastal ice in polar regions [Cota and Smith, 1991], and total biomass is about 2 orders of magnitude higher than in pack ice [Gosselin et al., 1997]. Because of the much smaller algal biomass present and its extensive vertical distribution through pack ice, focusing only on the ice algae at the bottom of pack ice will significantly underestimate biomass by a factor of at least 2 [Gradinger, 1999]. Thus analysis of the vertical structure of ice algae in the Arctic cannot be limited only to biomass in the bottom of the ice but must include different distributions for different ice types.

The reason for geographic differences in algal accumulation is likely linked to nutrient availability and perhaps grazing levels [Gradinger, 1999]. In coastal areas, algal growth has been strongly linked with the tidal current strength through its influence on the nutrient flux into the ice [Cota et al., 1987]. Since pack ice is not fixed to land, ice floes in the central Arctic may drift with water currents [Gradinger, 1999]. In addition, lower current velocities are observed in the central Arctic than are seen in the Canadian Arctic or Russian shelves [Kowalik and Proshutinsky, 1994]. These regional differences imply a lower current shear at the base of the pack ice, which results in a reduced influx of nutrients into the ice than that along the coasts [Gradinger, 1999].

#### 1.3.5 Bloom dynamics

Algal blooms last between 2 and 3 months in high latitudes and for about 6 weeks in the Subarctic [Cota et al., 1991]. The beginning of the bloom coincides with the return of sunlight in the spring, and normally declines after ice starts to melt in early summer [Cota and Smith, 1991]. Compared to higher latitudes, blooms at lower latitudes will start later, grow more slowly and terminate sooner because of shorter spring days and an earlier melt onset [Gosselin et al., 1985]. Following an initial exponential growth phase, biomass levels either plateau or oscillate before declining [Lavoie et al., 2005]. The reason for observed oscillations between algal growth and decline is still unclear [Fortier et al., 2002].

The rate of accumulation is also generally less with heavier snow covers [Cota and Smith, 1991]. The initiation of algal accumulation is thought to be largely controlled by snow thickness, because of its effect on light penetration [Fortier et al., 2002]. In general, in studies of bottom ice algae blooms in the Canadian Arctic, biomass levels can be determined based on snow depth observations [Cota and Smith, 1991]. Snow-free ice can have varying effects on the algal bloom, depending on when the snow disappears [Cota and Smith, 1991]. A study in the Canadian Arctic showed in that particular case that the biomass in areas with no snow cover accumulated at a normal rate but reached a lower peak level and declined earlier [Cota and Smith, 1991]. However, in the Canadian Arctic snow-free sea ice is not common [Welch and Bergmann, 1989].

The precise mechanisms determining the end of the bloom are unclear, but usually the end coincides with snow and bottom ice melt [Michel et al., 1996]. Thus if snow begins melting earlier in the season, the implication is that the ice algal bloom may be shorter [Fortier et al., 2002]. A more rapid snow melt

could also imply an accelerated discharge of algae and a faster rate of sinking [Lavoie et al., 2005]. Depending on atmospheric conditions such as the air temperature, the decline can be abrupt [Cota and Smith, 1991]. Since more biomass has been observed in ice that has low melt rates, it is possible that ice algae lost from melting at the ice base could be a cause of the bloom decline [Lavoie et al., 2005]. Melt at the base of the ice results in a deterioration of the platelet layer at the bottom of the ice where ice algae live, and also causes a melt water lens to form which increases stratification and reduces nutrient flux from the water column to the ice [Cota and Smith, 1991]. In the context of a warming Arctic, Fortier et al. [2002] suggest that more frequent early rain and hot spells will result in ice algae being more often dispelled out of the ice.

#### 1.3.6 Ice algae modeling

Very few ecosystem models include ice algae. Ice algae modeling in the past has mostly focused on a few locations in the Antarctic [Arrigo et al., 1993; Arrigo and Sullivan, 1994). A 1-D ice-ecosystem model for ice algal growth for McMurdo Sound, Antarctica was developed by [Arrigo et al., 1993]. Ice algae growth in this model is a function of temperature, spectral irradiance, nutrient concentration, and salinity [Arrigo et al., 1993]. Following what is commonly observed in coastal ice in McMurdo Sound, the model tracks ice algae inhabiting internal congelation ice, bottom congelation ice, and platelet ice microbial communities [Arrigo et al., 1993]. Although this model deals with the Antarctic, it provides a guide to determine what components to include in a model for Arctic ice. Its inclusion of salinity and brine dynamics as an influence on algal growth are worth considering when modeling central Arctic

ice, where ice algae are present more extensively in the column.

The model by Lavoie et al. [2005] models spring algal blooms in first year ice. It considers algae to be growing in the bottom 2 cm exclusively, with the upper water column supplying a flux of nutrients modulated by the tidal cycle. Algal growth depends on nutrient and light limitation, as well as a growth rate limitation used to handle the loss of algae from advection by the ice. Biomass is calculated using the growth rate, grazing rate, and algal loss due to ice melt. This model is used as a starting point for the coupled snow-ice-algae model presented here, with a more sophisticated snow-ice component allowing for improvement.

## 2 Model description

An adapted version of the bulk ice algae model of Lavoie et al. [2005] is coupled to the one-dimensional sigma-coordinate multi-layer thermodynamic model of Huwald et al. [2005]. The model employs a terrain-following coordinate system which includes a coordinate transformation in the governing heat conduction equation that naturally handles advection of ice. This allows for automatic re-layering and redistribution of energy between layers in an energy-conserving manner. As well the model allows for an arbitrary fixed number of layers in the snow and ice. Brine pockets in the ice are parameterized by taking into account salinity (S) as well as temperature (T) effects on the sea ice thermodynamic properties. The ice algae and nutrients in this model will be treated in a similar manner as other tracers in the model (T,S). Thus, while the focus of this paper is on algal blooms at the ice base, it is possible for ice algae to be present in the ice interior as well. Here a brief description of the thermodynamic snow ice model is included for completeness. More details of the thermodynamic equations can be found in Huwald et al. [2005].

## 2.1 Thermodynamic snow ice model

The conservation of mass equation for the snow/ice thickness (h) is written as:

$$\frac{\partial h}{\partial t} = S_h \tag{1}$$

where t is time and  $S_h$  represents a thermodynamic source or sink term. Following  $Huwald\ et\ al.$  [2005] I rewrite equation (1) in terms of the snow/ice

surface  $(s_s, s_i)$  and base elevations  $(b_i)$  as:

$$\frac{\partial s_s}{\partial t} = -(F_{net} + F_{cs})/(\rho_s L_f) , \quad \text{if } F_{net} + F_{cs} > 0 
+ p \cdot \rho_w/\rho_s , \quad \text{if } T_a \le 0^{\circ} C 
\frac{\partial s_i}{\partial t} = \begin{cases} -(F_{net} + F_{cs})/(\rho_i L_f) , & \text{if } F_{net} + F_{cs} > 0 \\ 0 , & \text{if } F_{net} + F_{cs} = 0 \end{cases} 
\frac{\partial b_i}{\partial t} = \frac{F_{ocn} + F_{cb}}{\rho_i L_f}$$

where subscripts 's' and 'i' denote snow and ice,  $F_{net}$  is the net atmospheric heat flux (radiative and turbulent) at the surface,  $F_{cs}$  and  $F_{cb}$  are the conductive heat fluxes at the snow/ice surface and ice base,  $\rho_i$ ,  $\rho_s$  and  $\rho_w$  are the density of ice, snow and freshwater (see Table 1), p is a precipitation rate,  $L_f$  is the specific latent heat of fusion,  $T_a$  is the air temperature, and  $F_{ocn}$  is the ocean heat flux at the ice base.

Following *Huwald et al.* [2005], I write the conservation of energy equation describing the temporal evolution of the snow and ice temperature as:

$$\rho \frac{\partial E}{\partial t} = \rho \left( \frac{\partial E}{\partial T} \frac{\partial T}{\partial t} + \frac{\partial E}{\partial S} \frac{\partial S}{\partial t} \right) = -\frac{\partial F_c}{\partial z} + R \tag{2}$$

where E is the internal energy of the sea ice brine mixture,  $F_c = -k(\partial T/\partial z)$  is the conductive heat flux in the snow or ice, and R is the absorbed shortwave energy per unit volume, defined using Beer's Law as:

$$R = \begin{cases} F_{ps} \kappa_s e^{-\kappa_s(s_s - z)}, & \text{for } b_s < z < s_s \\ F_{pi} \kappa_i e^{-\kappa_i(s_i - z)}, & \text{for } b_i < z < s_i \end{cases}$$
(3)

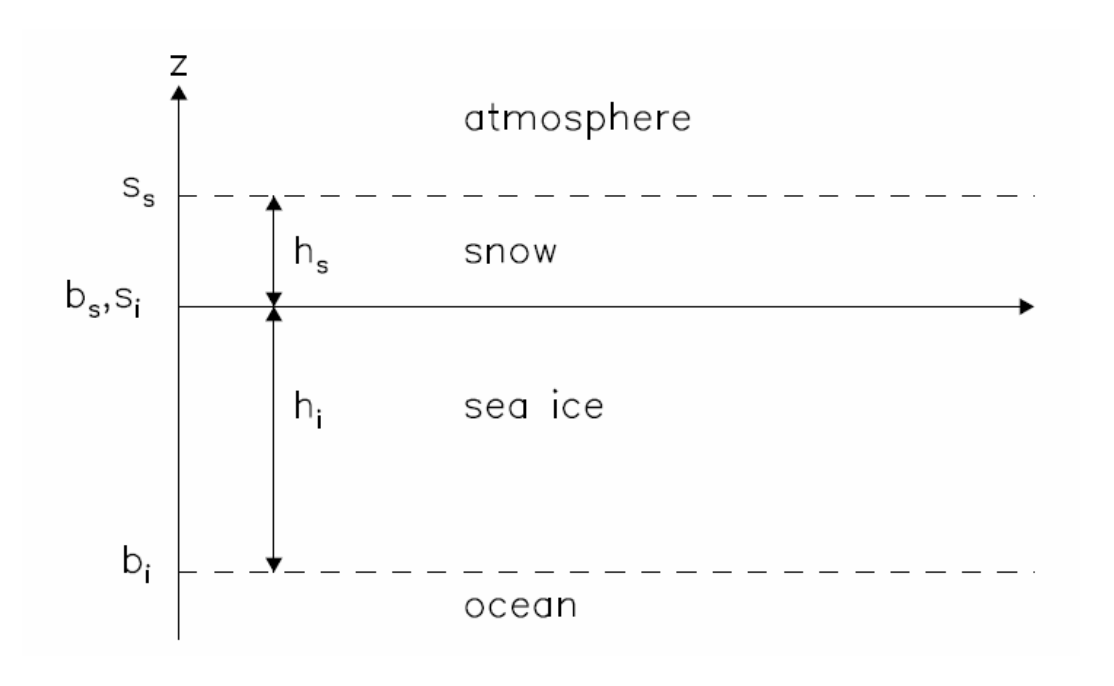


Figure 1: Sea ice model schematic. The letters s and b denote the surface and base, subscripts s and i stand for snow and ice, and  $h_s$ ,  $h_i$  are the snow and ice thickness respectively. The z-coordinate is positive upward (adapted from  $Huwald\ et\ al.\ [2005]$ ).

with

$$F_{ps}=F_{sw}(1-\alpha)i_0$$
 , at the snow or ice surface 
$$F_{pi}=F_{ps}e^{-\kappa_s h_s}$$
 , at the snow-ice interface

where  $F_{ps}$  and  $F_{pi}$  are the shortwave radiation at the snow surface and snowice interface respectively,  $\kappa_s$  and  $\kappa_i$  are the extinction coefficients for snow and ice,  $F_{sw}$  is the surface shortwave radiation,  $\alpha$  is the snow or ice albedo, and  $i_0$ is the surface transmission coefficient.

In this model  $F_{sw}$  is parameterized in terms of cloud cover, latitude, declination angle and other environmental variables [Parkinson and Washington, 1979]. Although  $\alpha$  is set as constant for snow or ice in Huwald et al. [2005], in this model it is parameterized using surface temperatures and ice thickness in an attempt to capture the changes in albedo over the melt season [Flato and

Brown, 1996. The parameterization is written as:

$$\alpha = \begin{cases} \alpha_{ow} , & \text{if } h_i < h_{min} \\ \min (\alpha_s , \alpha_i + h_s(\alpha_s - \alpha_i)/c_{10}) , & \text{if } h_i \ge h_{min} , h_s \le c_{10} \\ \alpha_s , & \text{if } h_i \ge h_{min} , h_s > c_{10} \end{cases}$$

where

$$\alpha_{i} = \begin{cases} \max \left(\alpha_{ow}, c_{11}h_{i}^{0.28} + 0.08\right), & \text{if } T(s_{i}, t) < T_{m} \\ \min \left(\alpha_{mi}, c_{12}h_{i}^{2} + \alpha_{ow}\right), & \text{if } T(s_{i}, t) = T_{m} \end{cases}$$

$$\alpha_{s} = \begin{cases} 0.75, & \text{if } T(s_{s}, t) < 0 \\ 0.65, & \text{if } T(s_{i}, t) = 0 \end{cases}$$

Refer to Table 1 for definitions and values of  $\alpha_{ow}$ ,  $\alpha_s$ ,  $\alpha_i$ ,  $\alpha_{mi}$ ,  $c_{10}$ ,  $c_{11}$ , and  $c_{12}$ .  $T_m$  is the melting temperature at the ice surface, defined as:

$$T_m = \mu_e S$$

where  $\mu_e = 0.054^{\circ} \text{C psu}^{-1}$ . This model considers salinity in the snow to be zero, so  $T_m$  of the snow surface is also zero.

Since changes in sea ice salinity occur on much larger time scales than changes in internal snow/ice temperature, I neglect the time derivative  $\partial S/\partial t$ , and equation (2) becomes:

$$\rho \frac{\partial E}{\partial t} = \rho c_p \frac{\partial T}{\partial t} = -\frac{\partial F_c}{\partial z} + R \tag{4}$$

In this model, the temperature and salinity dependent sea ice heat capacity

and bulk thermal conductivity are written following *Untersteiner* [1961]:

$$c_p(S,T) = c_{p0} + \frac{\gamma S}{T^2}$$
 and  $k_i(S,T) = k_{i0} + \frac{\beta S}{T}$ 

where  $c_{p0}$  and  $k_{i0}$  are the specific heat capacity and thermal conductivity of ice with zero salinity, and  $\beta$  and  $\gamma$  are empirical constants.

Table 1: Some physical parameters and constants in the snow ice model

| Symbol         | Definition  | Value                | Unit   |
|----------------|---|----------------------|--|
| $\alpha_i$     | albedo of ice   | calculated           |  |
| $\alpha_{ow}$  | albedo of open water  | 0.15                 |  |
| $\alpha_{mi}$  | albedo of melting ice   | 0.55                 |  |
| $\alpha_s$     | albedo of snow  | calculated           |  |
| $\beta$        | empirical constant  | 0.1172               | $\mathrm{Wm^{-1}\ psu^{-1}}$   |
| $c_{10}$       | parameter   | 0.1                  | m  |
| $c_{11}$       | parameter   | 0.44                 | $m^{-0.28}$  |
| $c_{12}$       | parameter   | 0.075                | $\mathrm{m}^{-2}$  |
| $\gamma$       | empirical constant  | $1.8 \times 10^{4}$  | $\mathrm{J}$ $^{o}\mathrm{C}$ $\mathrm{kg}^{-1}$ $\mathrm{psu}^{-1}$ |
| $c_{p0}$       | heat capacity of freshwater ice or snow                                 | $2.06 \times 10^{3}$ | $J kg^{-1} K^{-1}$   |
| $\vec{k}_{i0}$ | thermal conductivity of freshwater ice                                  | 2.03                 | ${ m Wm^{-1}~K^{-1}}$  |
| $i_0$          | fraction of net shortwave radiation penetrating the snow or ice surface | 0.5,  0.3            |  |
| $\kappa_i$     | bulk extinction coefficient of ice, non-melt to melt                    | 1.2 - 0.9            | $\mathrm{m}^{-1}$  |
| $\kappa_s$     | bulk extinction coefficient of snow, non-melt to melt                   | 14 - 7.5             | $\mathrm{m}^{-1}$  |
| $ ho_i$        | density of freshwater ice   | 917                  | ${\rm kg}~{\rm m}^{-3}$  |
| $ ho_s$        | density of snow   | 330                  | ${\rm kg}~{\rm m}^{-3}$  |
| $\rho_w$       | density of freshwater   | 1000                 | ${\rm kg}~{\rm m}^{-3}$  |

#### 2.1.1 Algae thermodynamic effects

Of the light absorbed by ice algae, only about 10% is used in photosynthesis, while the rest of the energy is released as heat [Lavoie et al., 2005]. Taking into account the absorption of shortwave energy by the ice algae, R (equation 3) is rewritten as:

$$R = \begin{cases} F_{ps} \kappa_s e^{-\kappa_s(s_s - z)}, & \text{for } b_s < z < s_s \\ F_{pi} (\kappa_i + fr \cdot \kappa_a) e^{-(\kappa_i + \kappa_a)(s_i - z)}, & \text{for } b_i < z < s_i \end{cases}$$

where  $F_{ps}$  remains unchanged since algae are generally not present in the snow, fr is the fraction of energy absorbed by the algae that is released as heat, and  $\kappa_a$  is the attenuation coefficient for algae, which varies linearly with the concentration of algae:

$$\kappa_a = a^* B$$

where  $a^*$  is the mean chl a-specific attenuation coefficient (0.02 m<sup>2</sup> mg chla<sup>-1</sup>, Kirk [1983]) and B (in mg chla m<sup>-3</sup>) is the concentration of chl a in the ice layer.

## 2.2 Ice algae - nutrient model

#### 2.2.1 Governing equations

Since silicon is generally considered the most limiting nutrient for ice algal growth [Cota and Horne, 1989; Cota et al., 1990; Smith et al., 1990], it is the nutrient included in this model. For the interior ice, the evolution equations for the biomass B (mg chla m<sup>-3</sup>) and the nutrient concentration of silicic acid N (mmol m<sup>-3</sup>) can be written as:

$$\frac{\partial B}{\partial t} = B\mu \tag{5}$$

$$\frac{\partial N}{\partial t} = -N_{up} \tag{6}$$

where  $\mu$  is the ice algal growth rate and  $N_{up}$  is the uptake rate of nutrient by the algae [Lavoie et al., 2005].

The ice algal growth rate  $\mu$  is calculated as:

$$\mu = \mu_{max} \min \left( N_{lim} , L_{lim} \right) \tag{7}$$

where  $\mu_{max}$  is a maximum temperature-dependent ice algal growth rate, and  $N_{lim}$  and  $L_{lim}$  are the nutrient and light limiting factors, respectively. Converting from day<sup>-1</sup> to sec<sup>-1</sup>,  $\mu_{max}$  is calculated after Eppley [1972]:

$$\mu_{max} = 86400 \cdot \log 2 \cdot (0.85e^{0.0633 T})$$

In equation (7),  $N_{lim}$  can be written as:

$$N_{lim} = \frac{N}{K_s + N} \tag{8}$$

where  $K_s$  is the half-saturation constant for Si(OH)<sub>4</sub> uptake (4 mmol m<sup>-3</sup>, Sarthou et al. [2005]), and  $L_{lim}$  is written as:

$$L_{lim} = tanh\left(\frac{\alpha^B R_{z_0}}{P_m^B}\right) \tag{9}$$

where  $\alpha^B$  is the photosynthetic efficiency,  $P_m^B$  is the maximum (light-saturated) photosynthetic rate of ice algae [Lavoie et al., 2005] and  $R_{z_0}$  is the shortwave radiation reaching the algae, obtained using Beer's Law.

The nutrient uptake rate by ice algae is given by:

$$N_{up} = \mu B \frac{N}{Chla} \tag{10}$$

where N/Chla = 10.3173 is the ratio (mmol Si:mg chl a) of silicate nutrient required to chl a produced [Lavoie et al., 2005].

#### 2.2.2 Platelet layer

Biomass at the ice base grows in thin platelets of ice forming a layer about 2 cm thick called the platelet layer [Maykut, 1985]. When calculating algal growth in this region, an additional growth factor G is included to take into account under-ice grazing. Grazing on the algae by other organisms is taken to be 10% of the growth rate  $[Lavoie\ et\ al.,\ 2005]$ :

$$\frac{\partial B}{\partial t} = B[\mu - G]$$

where  $G = 0.1\mu$ .

The principal source of nutrients for algae in the platelet layer is the ocean mixed layer, although other sources exist (such as through sea ice flushing).

While these other sources can become important for algal communities higher in the ice, they are not included in the present model. The nutrient flux  $(F_N)$  to the ice base depends on the nutrient concentration in the mixed layer and the thickness of the viscous sublayer. Following *Lavoie et al.* [2005] it is written as:

$$F_N = \frac{N_{mix} - N}{h_{tt}} D \tag{11}$$

where  $N_{mix} - N$  is the nutrient concentration gradient across the viscous sublayer of thickness  $h_{\nu}$ , and D (1 × 10<sup>-9</sup> m<sup>2</sup> s<sup>-1</sup>, Lavoie et al. [2005]) is the molecular diffusion coefficient of silicic acid. The nutrient concentration at the bottom of the viscous sublayer  $(N_{mix})$  is taken from observations. The nutrient equation in the platelet layer is then given by:

$$\frac{\partial N}{\partial t} = \frac{F_N}{dz_i} - N_{up} \tag{12}$$

where  $dz_i$  is the thickness of the platelet layer.

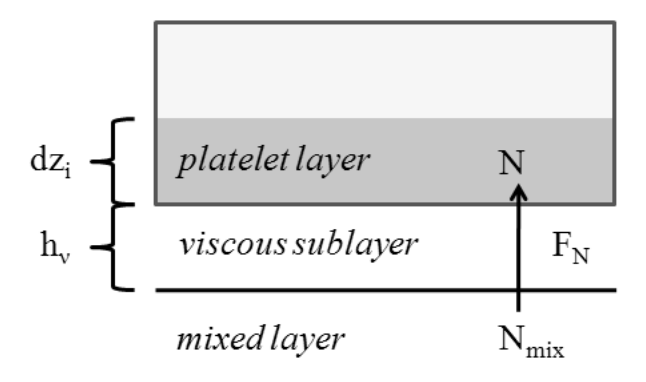


Figure 2: Schematic of nutrient concentrations and flux.

In equation (11), the viscous sublayer thickness is calculated after *Tennekes* and *Lumley* [1972]:

$$h_{\nu} = \frac{\nu}{u_{\tau}} \tag{13}$$

where  $\nu$  is the kinematic viscosity of seawater (1.85 × 10<sup>-6</sup> m<sup>2</sup> s<sup>-1</sup>) and  $u_{\tau}$  is the friction velocity.

## 2.3 Coordinate Transformation

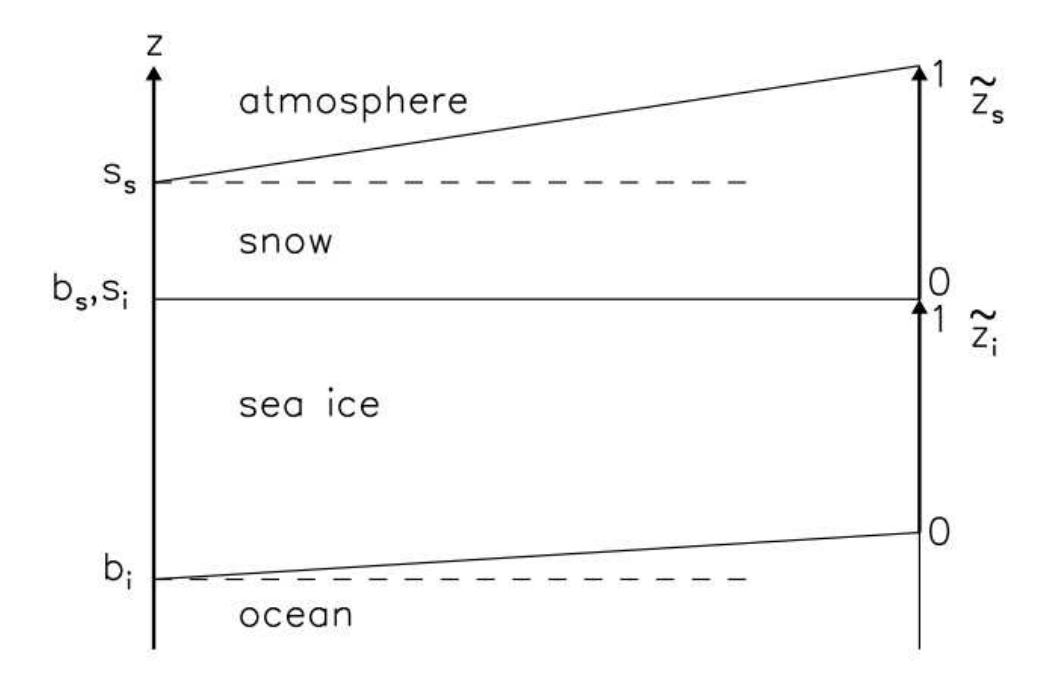


Figure 3: Coordinate transformation of the snow and ice components (adapted from *Huwald et al.* [2005])

#### 2.3.1 Thermodynamic model

Following Huwald et al. [2005], a coordinate transformation is applied for both the snow and ice, with the base and surface positioned at  $\tilde{z}=0$  and  $\tilde{z}=1$  (Figure 3):

$$\tilde{z} = \frac{z - b(t)}{s(t) - b(t)} = \frac{z - b(t)}{h(t)}$$
 and  $\tilde{t} = t$ 

where transformed variables are labelled with tilde.

Applying the chain rule to the conservation of energy equation, equation (2)

can be rewritten in terms of the transformed coordinate  $\tilde{z}$ :

$$\rho \left( \frac{\partial \tilde{E}}{\partial \tilde{t}} + \tilde{w} \frac{\partial \tilde{E}}{\partial \tilde{z}} \right) = \frac{1}{h^2} \frac{\partial}{\partial \tilde{z}} \left( k \frac{\partial \tilde{T}}{\partial \tilde{z}} \right) + \tilde{R}$$
 (14)

and

$$\tilde{w} = \frac{\partial \tilde{z}}{\partial \tilde{t}}$$

Note that  $\partial \tilde{t}/\partial t = 1$ . The continuity equation also remains unchanged by the transformation, as it is not a function of  $\tilde{z}$ . To get the energy equation in flux form, I multiply equation (14) by h and equation (1) by  $\tilde{E}$ , and then add them together:

$$\rho \left( h \frac{\partial \tilde{E}}{\partial \tilde{t}} + \tilde{E} \frac{\partial h}{\partial \tilde{t}} + \frac{\partial (\tilde{w}h\tilde{E})}{\partial \tilde{z}} \right) - \rho \tilde{E} \frac{\partial (\tilde{w}h)}{\partial \tilde{z}} = \frac{1}{h^2} \frac{\partial}{\partial \tilde{z}} \left( k \frac{\partial h\tilde{T}}{\partial \tilde{z}} \right) + h\tilde{R} + \rho \tilde{E} S_h$$
 (15)

Since thickness h does not depend on  $\tilde{z}$ , it can be taken inside the differential operator  $\partial/\partial \tilde{z}$ . Differentiating  $\tilde{w}$  with respect to  $\tilde{z}$  gives:

$$\frac{\partial \tilde{w}}{\partial \tilde{z}} = -\frac{1}{h} \left( \frac{\partial s}{\partial t} - \frac{\partial b}{\partial t} \right) = -\frac{1}{h} \frac{\partial h}{\partial t}$$
 (16)

$$\frac{\partial(\tilde{w}h)}{\partial\tilde{z}} = -\frac{\partial h}{\partial\tilde{t}} \tag{17}$$

Substituting equation (17) into equation (15) and using the continuity equation gives the final form of the transformed energy equations for snow and ice:

$$\rho\left(\frac{\partial(h_s\tilde{E}_s)}{\partial \tilde{t}} + \frac{\partial(\tilde{w}_s h_s\tilde{E}_s)}{\partial \tilde{z}_s}\right) = \frac{1}{h_s^2} \frac{\partial}{\partial \tilde{z}_s} \left(k_s \frac{\partial \theta_s}{\partial \tilde{z}_s}\right) + h_s\tilde{R}, \quad \text{for } 0 < \tilde{z}_s < 1$$

$$\rho\left(\frac{\partial(h_i\tilde{E}_i)}{\partial\tilde{t}} + \frac{\partial(\tilde{w}_ih_i\tilde{E}_i)}{\partial\tilde{z}_i}\right) = \frac{1}{h_i^2}\frac{\partial}{\partial\tilde{z}_i}\left(k_i\frac{\partial\theta_i}{\partial\tilde{z}_i}\right) + h_i\tilde{R}, \quad \text{for } 0 < \tilde{z}_i < 1$$

I also transform the radiative source and algae heat source terms. Thus equa-

tion (3) becomes:

$$\tilde{R} = \begin{cases} F_{ps} \kappa_s e^{-\kappa_s (1 - \tilde{z}_s) h_s}, & 0 < \tilde{z}_s < 1 \\ F_{pi} (\kappa_i + fr \cdot \kappa_a) e^{-(\kappa_i + \kappa_a)(1 - \tilde{z}_i) h_i}, & 0 < \tilde{z}_i < 1 \end{cases}$$

#### 2.3.2 Algae-nutrient model

I apply the same coordinate transformation to the algae and nutrient equations. The equations at the ice base are used here to show the flux and grazing terms in the new coordinate system. The equation for internal ice is also obtained by taking  $\tilde{F}_N = 0$  and G = 0. Thus, using the chain rule on equation (5) and (12) gives:

$$\frac{\partial \tilde{B}}{\partial \tilde{t}} \frac{\partial \tilde{t}}{\partial t} + \frac{\partial \tilde{B}}{\partial \tilde{z}} \frac{\partial \tilde{z}}{\partial t} = \tilde{B}[\tilde{\mu} - \tilde{G}]$$

$$\frac{\partial \tilde{N}}{\partial \tilde{t}} \frac{\partial \tilde{t}}{\partial t} + \frac{\partial \tilde{N}}{\partial \tilde{z}} \frac{\partial \tilde{z}}{\partial t} = \frac{\tilde{F}_N}{h \tilde{d} z} - \tilde{N}_{up}$$

where  $\tilde{\mu}$  is calculated with growth limitations in the new coordinate system:

$$\tilde{N}_{lim} = \frac{\tilde{N}}{K_s + \tilde{N}}$$

$$\tilde{L}_{lim} = tanh\left(\frac{\alpha^{\beta}\tilde{R}_{\tilde{z}_0}}{P_m^B}\right)$$

and

$$\tilde{N}_{up} = \tilde{\mu}\tilde{B}\frac{N}{Chla}$$

Substituting  $\tilde{w} = \partial \tilde{z}/\partial t$  gives:

$$\frac{\partial \tilde{B}}{\partial \tilde{t}} + \tilde{w} \frac{\partial \tilde{B}}{\partial \tilde{z}} = \tilde{B} [\tilde{\mu} - \tilde{G}]$$

and

$$\frac{\partial \tilde{N}}{\partial \tilde{t}} + \tilde{w} \frac{\partial \tilde{N}}{\partial \tilde{z}} = \frac{\tilde{F}_N}{h\tilde{d}z} - \tilde{N}_{up}$$

Using equation (17) and the continuity equation, as in the previous section, the transformed algae and nutrient equations in their final form are:

$$\frac{\partial(h_i\tilde{B})}{\partial\tilde{t}} + \frac{\partial(\tilde{w}h_i\tilde{B})}{\partial\tilde{z}_i} = h_i\tilde{B}[\tilde{\mu} - \tilde{G}]$$
(18)

$$\frac{\partial (h_i \tilde{N})}{\partial \tilde{t}} + \frac{\partial (\tilde{w} h_i \tilde{N})}{\partial \tilde{z}_i} = \frac{\tilde{F}_N}{\tilde{d} z_i} - h_i \tilde{N}_{up}$$
(19)

where  $0 < \tilde{z}_i < 1$ . Substituting  $\tilde{\gamma} = h_i \tilde{B}$  and  $\tilde{\xi} = h_i \tilde{N}$ , the transformed equations are given by:

$$\frac{\partial \tilde{\gamma}}{\partial \tilde{t}} + \frac{\partial (\tilde{w}\tilde{\gamma})}{\partial \tilde{z}_i} = \tilde{\gamma}[\tilde{\mu} - \tilde{G}]$$
 (20)

$$\frac{\partial \tilde{\xi}}{\partial \tilde{t}} + \frac{\partial (\tilde{w}\tilde{\xi})}{\partial \tilde{z}_i} = \frac{\tilde{F}_N}{\tilde{d}z_i} - h_i \tilde{N}_{up}$$
(21)

### 2.3.3 Internal algae advection

The coordinate transformation results in an advection term being added to the governing equations for algae and nutrients. While nutrients are advected through the ice in the same manner as other tracers (e.g. T or S), the behaviour of algae is somewhat different. When the ice growth rate is below a certain critical value  $w_{crit}$ , ice algae are able to keep their position at the bottom of the ice [Welch and Bergmann, 1989]. If the ice growth rate is larger than  $w_{crit}$ , the algae will be advected upwards. Although algae may similarly maintain their position during melt, other factors such as brine flushing will carry algae out of the ice during the melt season. Thus in the melting case, algae are

advected out of the ice in the same manner as other tracers. The advection velocity  $w_a$  in the algae equation can then be written as follows:

$$\frac{\partial \tilde{\gamma}}{\partial \tilde{t}} + \frac{\partial (\tilde{w_a}\tilde{\gamma})}{\partial \tilde{z}_i} = \tilde{\gamma}\tilde{\mu}$$

where:

$$w_a = max(w - |w_{crit}|, 0),$$
 for ice growth  $w_a = w,$  for ice melt

A value of 1.7 cm day<sup>-1</sup> is used for  $w_{crit}$  following Lavoie et al. [2005]. With an ice growth rate w that is slower than the critical growth rate, algae are able to maintain their position in the ice, while with a growth rate faster than  $w_{crit}$  algae are advected upward at a slowed rate.

### 2.3.4 Advection at the ice base

With the advection term appearing in the governing equations, a new boundary condition must be considered. When ice is growing, tracers are advected higher into the ice. Similarly, in the bottom layer we can decide whether the newly formed ice incorporates the nutrient concentration of the upper water column into its structure. Nutrients in the ice can be treated similarly to salt, since the pure ice itself is virtually free of impurities and all nutrients and salts are considered to be dissolved within brine inclusions [Krembs et al., 2001]. When ice is first formed, salt is included in its structure; however a rapid desalination stage follows shortly afterward [Vancoppenolle et al., 2007]. The model presented here does not yet include brine flushing dynamics that can describe this expulsion of salt and nutrients. I therefore consider the nutrient concentration incorporated into the growing bottom layer to be equal to zero.

The diffusive nutrient flux described in section 2.2.2 remains the provider of nutrients into the base of the ice. This flux is not affected by whether the ice is growing or melting. While it is a good starting point, the supply of nutrients in the model may be improved in the future by taking into account nutrient incorporation associated with brine rejection and stratification from meltwater during melt. At present, nutrients may continue to enter the ice during melt through the diffusive flux, while nutrients in the ice are lost through advection downward. By the same argument, ice algae concentration in newly formed ice is also assumed to be zero.

## 2.4 Numerical scheme

The equations are:

$$\frac{\partial \tilde{\gamma}}{\partial \tilde{t}} + \frac{\partial (\tilde{w}_a \tilde{\gamma})}{\partial \tilde{z}_i} = \tilde{\gamma} \tilde{\mu}$$
 (22)

$$\frac{\partial \tilde{\xi}}{\partial \tilde{t}} + \frac{\partial (\tilde{w}\tilde{\xi})}{\partial \tilde{z}_i} = h_i \tilde{S}$$
 (23)

where 
$$\tilde{S} = -\tilde{N}_{up}$$

The terms in the transformed algae and nutrient equations are treated similarly to the terms in the energy equation. The time derivative is discretized using a forward step and the advection term is evaluated implicitly using an energy-conserving first order upstream scheme. Equations (22) and (23) can be written as a linear, inhomogeneous system:

$$A_j^{t+1} \tilde{\gamma}_{j-1}^{t+1} + B_j^{t+1} \tilde{\gamma}_j^{t+1} + C_j^{t+1} \tilde{\gamma}_{j+1}^{t+1} = D_j^t$$

$$E_j^{t+1}\tilde{\xi}_{j-1}^{t+1} + F_j^{t+1}\tilde{\xi}_j^{t+1} + G_j^{t+1}\tilde{\xi}_{j+1}^{t+1} = H_j^t$$

These equations can be written in matrix form:

$$\begin{pmatrix} & \ddots & & \\ A_{j-1} & B_{j-1} & C_{j-1} & & \\ & A_{j} & B_{j} & C_{j} & \\ & & A_{j+1} & B_{j+1} & C_{j+1} \\ & & & \ddots & \end{pmatrix} \begin{pmatrix} \tilde{\gamma}_{0} \\ \tilde{\gamma}_{1} \\ \vdots \\ \tilde{\gamma}_{j-1} \\ \tilde{\gamma}_{j} \\ \tilde{\gamma}_{j+1} \\ \vdots \\ \tilde{\gamma}_{N} \end{pmatrix} = \begin{pmatrix} D_{0} \\ D_{1} \\ \vdots \\ D_{j-1} \\ D_{j} \\ D_{j+1} \\ \vdots \\ D_{N} \end{pmatrix}$$

and

$$\begin{pmatrix} & \ddots & & & \\ E_{j-1} & F_{j-1} & G_{j-1} & & & \\ & E_{j} & F_{j} & G_{j} & & \\ & & E_{j+1} & F_{j+1} & G_{j+1} \\ & & & \ddots & \end{pmatrix} \begin{pmatrix} \tilde{\xi}_{0} \\ \tilde{\xi}_{1} \\ \vdots \\ \tilde{\xi}_{j-1} \\ \tilde{\xi}_{j} \\ \tilde{\xi}_{j+1} \\ \vdots \\ \tilde{\xi}_{N} \end{pmatrix} = \begin{pmatrix} H_{0} \\ H_{1} \\ \vdots \\ H_{j-1} \\ H_{j} \\ H_{j+1} \\ \vdots \\ H_{N} \end{pmatrix}$$

## 2.4.1 Internal layers

$$(2 \le j \le N)$$

Consider the algae equation. The subscript for  $w_a$  is dropped to simplify the notation. For  $\tilde{w}_j$ ,  $\tilde{w}_{j+1} > 0$ :

numerator of time derivative (NTD)<sub>j</sub> numerator of advection term (NAT1)<sub>j</sub> 
$$\frac{\tilde{\gamma}_{j}^{t+1} - \tilde{\gamma}_{j}^{t}}{\Delta \tilde{t}} + \frac{\tilde{w}_{j+1}^{t+1} \tilde{\gamma}_{j}^{t+1} - \tilde{w}_{j}^{t+1} \tilde{\gamma}_{j-1}^{t+1}}{\Delta \tilde{z}} = (\tilde{\mu} \tilde{\gamma})_{j}^{t+1}$$

For  $\tilde{w}_j$ ,  $\tilde{w}_{j+1} < 0$ :

numerator of time derivative (NTD)\_j numerator of advection term (NAT2)\_j 
$$\underbrace{ \frac{\tilde{\gamma}_j^{t+1} - \tilde{\gamma}_j^t}{\Lambda \tilde{t}}}_{\Lambda \tilde{t}} + \underbrace{ \frac{\tilde{w}_{j+1}^{t+1} \tilde{\gamma}_{j+1}^{t+1} - \tilde{w}_j^{t+1} \tilde{\gamma}_j^{t+1}}{\Lambda \tilde{z}}}_{\text{numerator of advection term (NAT2)_j} = (\tilde{\mu} \tilde{\gamma})_j^{t+1}$$

which written in shorthand gives:

$$(\text{NTD})_{j} = -\frac{\Delta \tilde{t}}{\Delta \tilde{z}} (\text{NAT1})_{j} + \Delta \tilde{t} (\tilde{\mu} \tilde{\gamma})_{j}^{t+1} \qquad \tilde{w}_{j} > 0$$
  
$$(\text{NTD})_{j} = -\frac{\Delta \tilde{t}}{\Delta \tilde{z}} (\text{NAT2})_{j} + \Delta \tilde{t} (\tilde{\mu} \tilde{\gamma})_{j}^{t+1} \qquad \tilde{w}_{j} < 0$$

Define coefficients:

$$C1^{t+1} = \frac{\Delta \tilde{t}}{\Delta \tilde{z}}$$
  $C2^{t+1} = \Delta \tilde{t} \tilde{\mu}_j^{t+1}$ 

$$(NTD)_j + C1(NAT1)_j = C2(\tilde{\gamma})_j$$
  $\tilde{w}_j > 0$   
 $(NTD)_j + C1(NAT2)_j = C2(\tilde{\gamma})_j$   $\tilde{w}_j < 0$ 

Thus, for  $\tilde{w}_j$ ,  $\tilde{w}_{j+1} > 0$ :

$$\tilde{\gamma}_{j}^{t+1} - \tilde{\gamma}_{j}^{t} + C1\tilde{w}_{j+1}^{t+1}\tilde{\gamma}_{j}^{t+1} - C1\tilde{w}_{j}^{t+1}\tilde{\gamma}_{j-1}^{t+1} = C2(\tilde{\gamma})_{j}^{t+1}$$

$$\underbrace{\left(-C1\tilde{w}_{j}^{t+1}\right)}_{A_{j}}\tilde{\gamma}_{j-1}^{t+1} + \underbrace{\left(1 + C1\tilde{w}_{j+1}^{t+1} - C2\right)}_{B_{j}}\tilde{\gamma}_{j}^{t+1} + \underbrace{\left(0\right)}_{C_{j}}\tilde{\gamma}_{j+1}^{t+1} = \underbrace{\tilde{\gamma}_{j}^{t}}_{D_{j}}$$

and for  $\tilde{w}_j$ ,  $\tilde{w}_{j+1} < 0$ :

$$\tilde{\gamma}_{j}^{t+1} - \tilde{\gamma}_{j}^{t} + C1\tilde{w}_{j+1}^{t+1}\tilde{\gamma}_{j+1}^{t+1} - C1\tilde{w}_{j}^{t+1}\tilde{\gamma}_{j}^{t+1} = C2(\tilde{\gamma})_{j}^{t+1}$$

$$\underbrace{(0)}_{A_j} \tilde{\gamma}_{j-1}^{t+1} + \underbrace{\left(1 - \mathbf{C}1\tilde{w}_j^{t+1} - \mathbf{C}2\right)}_{B_j} \tilde{\gamma}_j^{t+1} + \underbrace{\left(\mathbf{C}1\tilde{w}_{j+1}^{t+1}\right)}_{C_j} \tilde{\gamma}_{j+1}^{t+1} = \underbrace{\tilde{\gamma}_j^t}_{D_j}$$

The nutrient equation is handled slightly differently, since an N term does not appear on the righthand side of the equation. In this case, for  $\tilde{w}_j$ ,  $\tilde{w}_{j+1} > 0$ :

numerator of time derivative (NTD)\_j numerator of advection term (NAT1)\_j 
$$\underbrace{\frac{\tilde{\xi}_j^{t+1} - \tilde{\xi}_j^t}{\Lambda \tilde{t}}}_{} + \underbrace{\frac{\tilde{w}_{j+1}^{t+1} \tilde{\xi}_j^{t+1} - \tilde{w}_j^{t+1} \tilde{\xi}_{j-1}^{t+1}}{\Lambda \tilde{z}}}_{} = h_i \tilde{S}_j^{t+1}$$

and for  $\tilde{w}_j$ ,  $\tilde{w}_{j+1} < 0$ :

$$\underbrace{\frac{\tilde{\xi}_{j}^{t+1} - \tilde{\xi}_{j}^{t}}{\Delta \tilde{t}}}_{\text{numerator of advection term (NAT2)}_{j} + \underbrace{\frac{\tilde{w}_{j+1}^{t+1} \tilde{\xi}_{j+1}^{t+1} - \tilde{w}_{j}^{t+1} \tilde{\xi}_{j}^{t+1}}{\Delta \tilde{z}}}_{\text{numerator of advection term (NAT2)}_{j} = h_{i} \tilde{S}_{j}^{t+1}$$

Another coefficient is defined:

$$C3^{t+1} = h_i \Delta \tilde{t}$$

Thus for  $\tilde{w}_j$ ,  $\tilde{w}_{j+1} > 0$ :

$$\tilde{\xi}_{j}^{t+1} - \tilde{\xi}_{j}^{t} + C1\tilde{w}_{j+1}^{t+1}\tilde{\xi}_{j}^{t+1} - C1\tilde{w}_{j}^{t+1}\tilde{\xi}_{j-1}^{t+1} = C3(\tilde{S})_{j}^{t+1}$$

$$\underbrace{\left(-C1\tilde{w}_{j}^{t+1}\right)}_{E_{j}}\tilde{\xi}_{j-1}^{t+1} + \underbrace{\left(1 + C1\tilde{w}_{j+1}^{t+1}\right)}_{F_{j}}\tilde{\xi}_{j}^{t+1} + \underbrace{\left(0\right)}_{G_{j}}\tilde{\xi}_{j+1}^{t+1} = \underbrace{C3(\tilde{S})_{j}^{t+1} + \tilde{\xi}_{j}^{t}}_{H_{j}}$$

For  $\tilde{w}_j$ ,  $\tilde{w}_{j+1} < 0$ :

$$\tilde{\xi}_{j}^{t+1} - \tilde{\xi}_{j}^{t} + \text{C1}\tilde{w}_{j+1}^{t+1}\tilde{\xi}_{j+1}^{t+1} - \text{C1}\tilde{w}_{j}^{t+1}\tilde{\xi}_{j}^{t+1} = \text{C3}(\tilde{S})_{j}^{t+1}$$

$$\underbrace{(0)}_{E_{j}}\tilde{\xi}_{j-1}^{t+1} + \underbrace{\left(1 - \text{C1}\tilde{w}_{j}^{t+1}\right)}_{F_{j}}\tilde{\xi}_{j}^{t+1} + \underbrace{\left(\text{C1}\tilde{w}_{j+1}^{t+1}\right)}_{G_{j}}\tilde{\xi}_{j+1}^{t+1} = \underbrace{\text{C3}(\tilde{S})_{j}^{t+1} + \tilde{\xi}_{j}^{t}}_{H_{j}}$$

### 2.4.2 Bottom ice layer

$$(j = 1)$$

Algae in the bottom (i.e. platelet) layer follow the formulation given for the internal layers, but the nutrient flux from the water column must be included in the nutrient equation.

For  $\tilde{w}_1, \tilde{w}_2 > 0$ :

$$\frac{\tilde{\xi}_1^{t+1} - \tilde{\xi}_1^t}{\Delta \tilde{t}} + \frac{\tilde{w}_2^{t+1} \tilde{\xi}_1^{t+1} - \tilde{w}_1^{t+1} \tilde{\xi}_0^{t+1}}{\Delta \tilde{z}} = \left( h_i \tilde{S} + h_i \frac{N_{mix} - N}{h_{\nu} \tilde{dz}_i h_i} D \right)_1^{t+1}$$

$$\underbrace{\left(-\text{C1}\tilde{w}_{1}^{t+1}\right)}_{E_{1}}\tilde{\xi}_{0}^{t+1} + \underbrace{\left(1+\text{C1}\tilde{w}_{2}^{t+1} + \frac{D\Delta t}{h_{\nu}\tilde{dz}_{i}h_{i}}\right)}_{F_{1}}\tilde{\xi}_{1}^{t+1} + \underbrace{0}_{G_{1}} = \underbrace{\text{C3}\tilde{S}_{1}^{t+1} + \frac{D\Delta t}{h_{\nu}\tilde{dz}_{i}}N_{mix}}_{H_{1}}^{t+1} + \underbrace{\tilde{\xi}_{1}^{t}}_{H_{1}}$$

For  $\tilde{w}_1, \tilde{w}_2 < 0$ :

$$\frac{\tilde{\xi}_{1}^{t+1} - \tilde{\xi}_{1}^{t}}{\Delta \tilde{t}} + \frac{\tilde{w}_{2}^{t+1} \tilde{\xi}_{2}^{t+1} - \tilde{w}_{1}^{t+1} \tilde{\xi}_{1}^{t+1}}{\Delta \tilde{z}} = \left(h_{i} \tilde{S} + h_{i} \frac{N_{mix} - N}{h_{\nu} \tilde{d} z_{i} h_{i}} D\right)_{1}^{t+1}$$

$$\underbrace{0}_{E_1} \tilde{\xi}_0^{t+1} + \underbrace{\left(1 - C1\tilde{w}_1^{t+1} + \frac{D\Delta t}{h_{\nu}\tilde{dz}_i h_i}\right)}_{F_1} \tilde{\xi}_1^{t+1} + \underbrace{C1\tilde{w}_2^{t+1}}_{G_1} \tilde{\xi}_2^{t+1} = \underbrace{C3\tilde{S}_1^{t+1} + \frac{D\Delta t}{h_{\nu}\tilde{dz}_i} N_{mix}}_{H_1}^{t+1} + \underbrace{\tilde{\xi}_1^t}_{H_1}$$

## **2.4.3** Ice base

$$(j = 0)$$

With no algae and nutrients incorporated into the ice base during growth, and losses during melt through advection, the bottom boundary condition at j=0 is given by B=0 and N=0.

For  $\tilde{w}_1 > 0$  and  $\tilde{w}_1 < 0$ 

$$\underbrace{1}_{B_0} \tilde{\gamma}_0^{t+1} + \underbrace{(0)}_{C_0} \tilde{\gamma}_1^{t+1} = \underbrace{0}_{D_0}$$

$$\underbrace{1}_{F_0} \tilde{\xi}_0^{t+1} + \underbrace{(0)}_{G_0} \tilde{\xi}_1^{t+1} = \underbrace{0}_{H_0}$$

# 3 Data

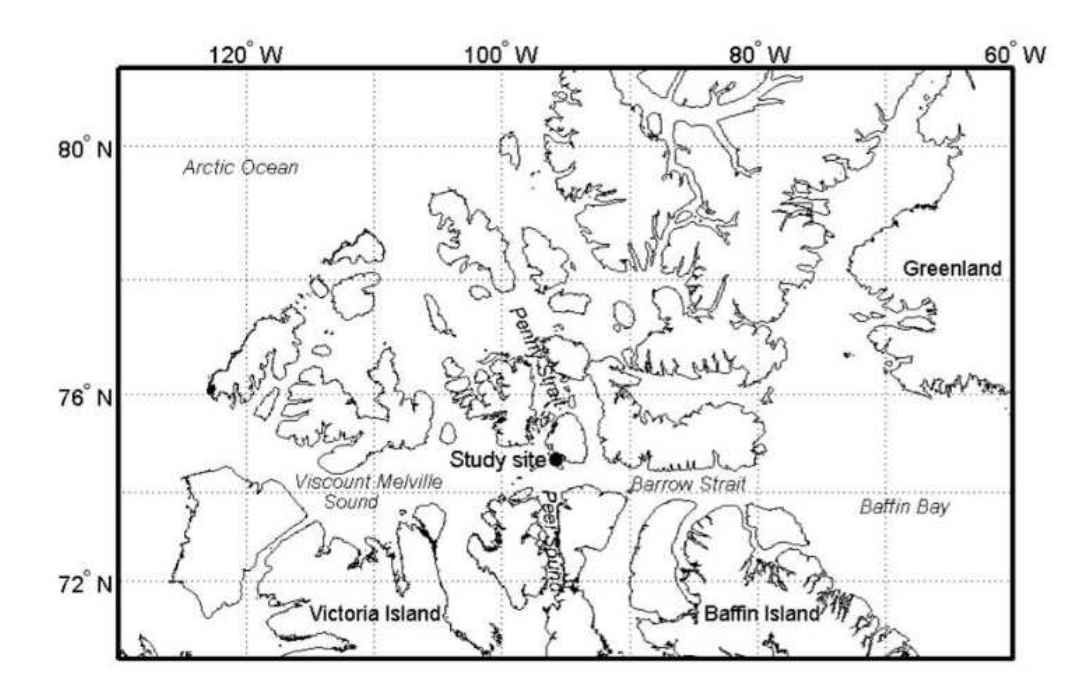


Figure 4: Location of study site (adapted from Lavoie et al. [2005]).

Data for this study were provided by Christine Michel and Rick Marsden, from field observations taken in the spring (mid-May to early July) of 2002 at a landfast ice station in Resolute Passage (74°42.5'N) near Barrow Strait in the Canadian Arctic Archipelago. In this area, the polar night lasts from November to early February. Surface waters flowing through this area are nutrient-rich and of Pacific origin, and the water depth at the sampling station was 120 m. Although the water column properties are relatively well mixed, tidal modulation does cause some variability in the stratification.

Meteorological data including wind, air temperature and relative humidity, were taken at the sampling station, and cloud cover fraction data was obtained from an Environment Canada station located about 30km southeast of the sampling site. Under-ice temperature was measured every 5 minutes by a Sea-Bird SBE37 probe moored at 1 m below the ice. Nutrient data was taken from

water column samples collected using Niskin bottles at four depths (2.5, 5, 10 and 25 m) at 3- to 4-day intervals.

Measurements of under-ice photosynthetically availabe radiation (PAR, 400-700 nm) were taken every 15 minutes using a LiCOR quantum sensor located at 0.5 m underneath the ice, and connected to a LiCOR 1400 data logger. Daily snow thickness data was also obtained at this "PAR" site. Ice algae were sampled at two sites with different snow thicknesses (roughly 20 cm and 10 cm), denoted the high snow cover (HSC) and low snow cover (LSC) sites. Algae samples were taken every 3 to 4 days from the bottom 2-4 cm of an ice core made using a MARK II coring system. Coring positions were chosen where snow thickness was close to 10 or 20 cm, resulting in some spatial variability with the algae samples. Ice thickness data was also recorded at this time, as well as snow thickness. A complete description of the data set can be found in Lavoie et al. [2005].

# 4 Results and Discussion

The model was run during the 2002 spring bloom, from julian days 130 (May 10) to 182 (July 1) for each of the three data sites (PAR, HSC, LSC), with a 15 minute timestep. The number of snow layers used by the model is 12, and the number of ice layers is 55. This results in a bottom ice layer initial thickness of approximately 3 cm (approximately the thickness where most of the biomass was observed). The model was initialized with zero ice algae in all layers except the bottom ice layer (set to 300 mg chla m<sup>-3</sup> and 700 mg chla m<sup>-3</sup> for the HSC and LSC sites, respectively), according to observations. Snow and ice thicknesses in the model were initially set to observed values on May 10. Observations were used to prescribe the snow thickness of the model except during melting, when it was calculated. For each site two simulations were run, one with the brine parameterization included and one without. Taking into account the thermodynamic effect of brine pockets is more physically sound, and so I focus our analysis on this model run (henceforth referred to as the "brine run").

The photosynthetic parameters  $\alpha^B$  and  $P_m^B$  (defined in section 2.2.1) vary from site to site. In the following I use values chosen by *Lavoie et al.* [2005] based on in situ measurements. The values for the three observation sites are shown in Table 2.

Table 2: Photosynthetic parameters for the 3 data sites

| $\alpha^B$ | $P_m^B$ |
|------------|---------|
| 0.055      | 0.285   |
| 0.03       | 0.3     |
| 0.12       | 0.27    |
|            | 0.055   |

## 4.1 Ice/snow thickness comparison

Correctly simulating the ice thickness is important, because of its effect on PAR reaching the ice algae and on algal loss through basal melt. The comparison of the simulated and observed ice/snow thickness at the HSC and LSC sites is shown in Figure 5. The snow thickness simulated by the model (during the melt phase) is in close agreement with the interpolated snow thickness observations at both sites. A small discrepancy in the snow thickness exists at the LSC site after day 167, at which point melt was calculated by the model at both sites. This difference was most likely because of blowing snow that the model did not take into account. Overall the simulated ice thickness closely matches the observations. The model simulates an increased rate of ice melt in the last 10 days, as is expected as the snow cover disappears. Although snow and ice thickness data is available over the entire study period at the LSC site, data at the HSC site does not extend past day 170, when snow cover is completely gone. As a result, the accelerated ice melt occurring over the last 10 days of the period cannot be compared to observations at the HSC site. Because of the moderating effect of the brine pockets during ice melt, the brine run has a slower melt. This simulation appears to be a closer fit to the observations, although the lack of observations later in the season makes it difficult to confidently assess this fact. However, Figure 5 shows that at the LSC site the simulated ice thickness of the brine model run fits the data well.

### 4.2 PAR at the ice base

Given the strong dependence of ice algae growth on light levels, it is important to ensure that the shortwave radiation absorbed and transmitted through the ice is accurately modeled. In the following, I compare simulated short-

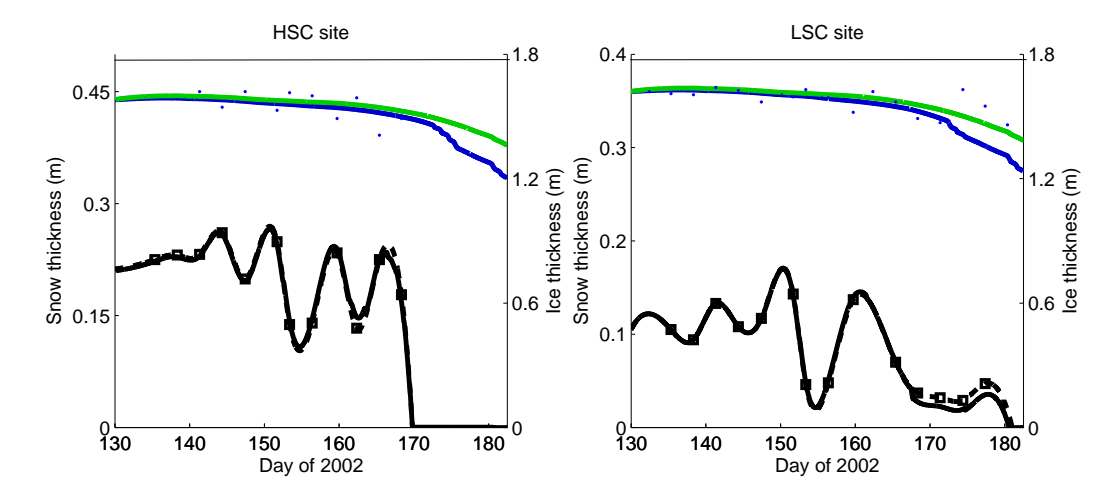


Figure 5: Observed (blue dots) and simulated ice thicknesses with (green line) and without (blue line) brine, and observed (black squares) and interpolated snow thickness (solid black line) compared to simulated snow thickness (dashed black line), at HSC (left panel) and LSC sites (right panel).

wave radiation reaching the ice base to the under-ice PAR data measured by Michel (2002). This data is used to validate the light attenuation ( $\kappa_s$ ,  $\kappa_i$ ) and penetrating coefficients ( $i_0$ ) used in the subsequent model/data comparison discussed in section 4.3. The absorption of shortwave radiation in sea ice is 3-13 times larger for wavelengths longer than 700 nm than it is for the visible range [Grenfell and Maykut, 1977]. It is for this reason that I assume, as in Zeebe et al. [1996], that only the visible range (400-700 nm) penetrates the ice interior, while longer wavelengths are absorbed within the surface layer. Thus I can directly compare observed under-ice PAR with simulated shortwave radiation, which is henceforth referred to as simulated PAR.

The amount of PAR penetrating the ice base is dependent on the light attenuation and penetrating coefficients used by the model. When a lower value of  $i_0$  is used, more shortwave radiation is absorbed directly at the snow or ice surface. Following *Grenfell and Maykut* [1977], I use an average value of 0.5 for first year ice. Much less light penetrates through snow, and in past model studies, values of  $i_0$  for snow range from 0 to 0.08 [*Huwald et al.*, 2005;

Ohmura, 1984]. Using such low values for this parameter, however, will result in little to no PAR reaching the base of the ice over the study period (contrary to observations). As melt occurs, more light penetrates through ice and snow [Grenfell and Maykut, 1977], suggesting that while values below 0.1 may be appropriate for drier snow, a higher value may be needed for the melt season. To the author's knowledge however, no detailed measurements of  $i_0$  for different snow conditions exist in the literature. In this study, I adopt a value of  $i_0$  for snow equal to 0.3.

The attenuation coefficients used in the model for dry snow  $\kappa_s$  and cold ice  $\kappa_i$  are 14 m<sup>-1</sup> and 1.2 m<sup>-1</sup>, respectively [Grenfell and Maykut, 1977; Smith et al., 1988]. For melting snow and ice,  $\kappa_s$  and  $\kappa_i$  have values of 7.5 m<sup>-1</sup> [Grenfell and Maykut, 1977] and 0.9 m<sup>-1</sup> [Light et al., 2008], respectively. In the model,  $\kappa_s$  and  $\kappa_i$  are initially set to the higher, cold season values. When melting is initiated (calculated in the model as when surface temperature is at melting point and the net heat flux at the surface is directed into the ice),  $\kappa_s$  and  $\kappa_i$  incrementally decrease by  $3 \times 10^{-4}$  every 15 minutes until the melt season values listed above are reached.

Figure 6 shows a comparison between the simulated and observed under-ice PAR over the study period. Simulated snow/ice thickness and algae are also plotted, because these parameters have an affect on available under-ice PAR as well. Ideally, ice thickness measurements would be used for comparison at the PAR site to ensure that discrepancies between observed and simulated PAR are not because of an inaccurately modeled ice thickness. Ice thickness observations from the HSC and LSC sites can be used as guidelines, however.

The evolution of the snow/ice thickness for both cases is plotted in Figure 6b. With the thicker ice cover in the brine model run, light reaching the ice base

is more strongly attenuated in that simulation (Figure 6a). After day 170 the snow is completely gone, exposing the ice to surface temperatures and accelerating ice melt (Figure 6b and 6c). The disappearance of the light-blocking snow cover also explains the rapid increase in under-ice PAR seen in Figure 6a. Algae was included in the model runs for this site to take into account the attenuation of light by the algae itself (Figure 6d). Since algal samples were not taken at the PAR site, the model output of biomass was compared to samples taken at the LSC and HSC sites. The biomass simulated at the PAR site varies between the data sets of the 2 sites, providing a reasonable range of values.

Differences exist between simulated and observed under-ice PAR after day 165 (Figure 6a). This inconsistency is likely because of the choice for  $\kappa_i$ , since snow depth is zero after that time. This parameter can vary depending on ice conditions, and a temperature-based parameterization over a range of values is likely a more appropriate choice. The ice algae growth rate is not affected by this discrepancy between simulated and observed values however, since the algae is not light limited at the end of the bloom (see next section, Figure 7b).

# 4.3 Algal bloom

At the HSC site the bloom begins with a significant light limitation under a thicker snow cover (Figure 7a) when compared to the LSC site (Figure 7b). Even though more light initially reaches the base of the ice at the LSC site, differing adaptation by the algae to light conditions at the sites (described using photosynthetic parameters  $\alpha^B$  and  $P_m^B$  - see Table 2) results in similarly low initial light limitations (equation 9). As well, the light limitation curve at both sites follows an oscillatory pattern driven by the snow depth profile, with

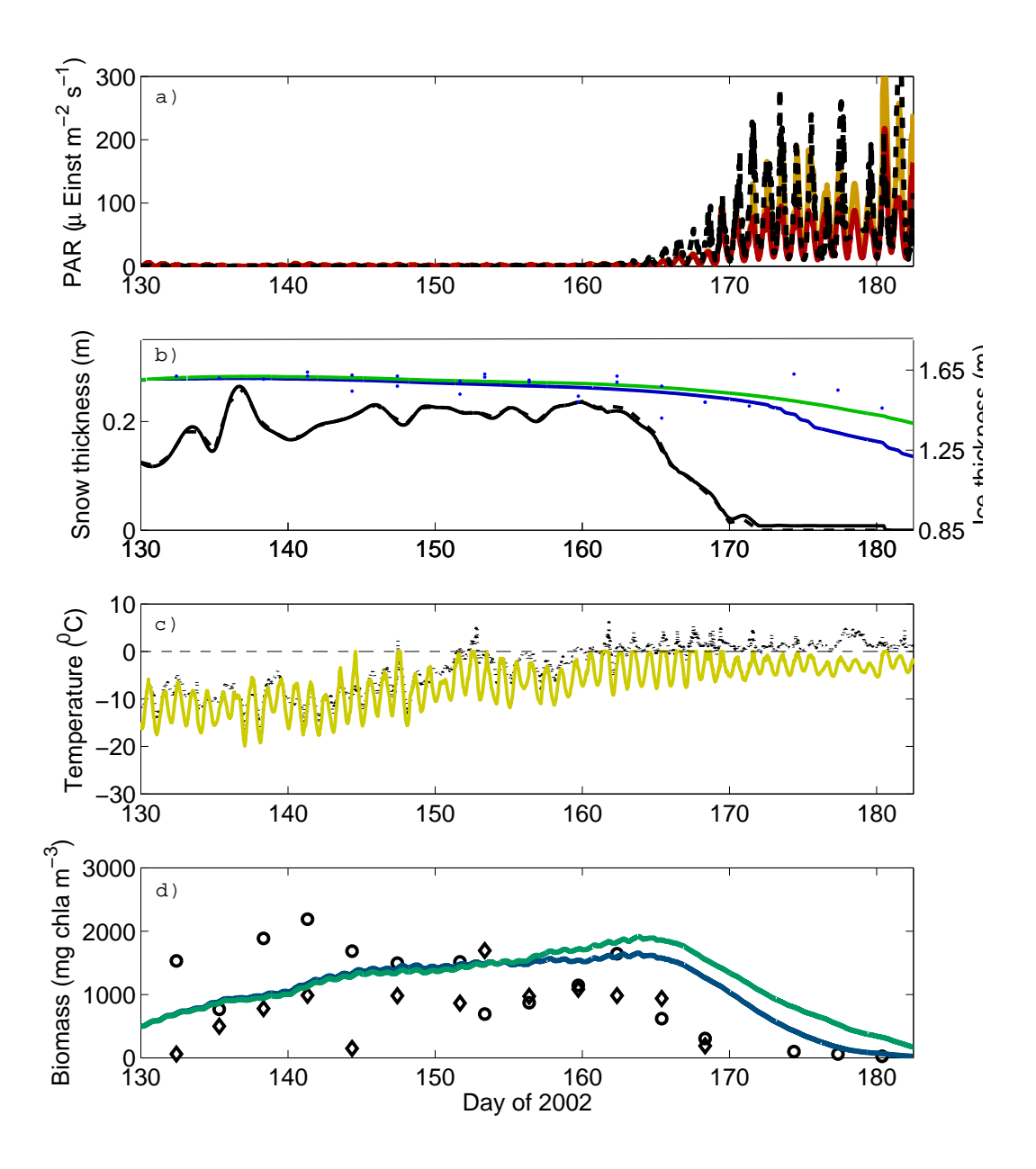


Figure 6: Time series of a) observed under-ice PAR (black dashed line) compared with simulated values with (red line) and without brine (orange line), b) observed (black dashed line) and simulated (solid black line) snow thickness and simulated ice thickness with (green line) and without brine (blue line) and ice thickness observed at the HSC and LSC sites (blue dots), c) hourly mean observed air temperature at 2 m (black dashed line) and simulated surface temperature (yellow line) with brine, and d) simulated chl a biomass with (green line) and without brine (blue line) compared with observed biomass at the LSC (black circles) and HSC sites (black diamonds).

light availability peaking during periods of minimum snow depth. Around the middle of the bloom (day 150-160), the algae transitions into a nutrient limitation phase as more light penetrates the thinner ice cover. After day 151 the largest decrease in snow depth occurs at both sites (Figure 5), allowing more light to reach the algae at the base of the ice (Figure 7c and 7d). This heightened light availability causes a spurt in algal growth, in turn increasing the uptake of nutrients and resulting in a nutrient depletion (see Figure 7b, 7b and 9). A nutrient limitation remains over the rest of the bloom, but the nutrient supply recovers as the biomass declines at the end of the bloom season (Figure 9). Nutrient concentration in the ice (Figure 9) and algal growth (Figure 8) both oscillate (following the diurnal cycle) in periods of the bloom when light is limiting growth. When the snow depth reaches zero around day 171, there is ample light available. These results are in agreement with Lavoie et al. [2005] in their pattern of light and nutrient limitations.

Figure 7c and 7d show the temporal evolution of ice algae biomass during the bloom, as well as available PAR in the bottom layer. Algae remains in the bottom layer of the model over the simulation, because  $w_{max}$  allows the algae to maintain their position during ice growth in the early bloom stage. When comparing the two model simulations with and without the brine parameterization, it is interesting to see that despite overall having lower light conditions under a thicker ice cover, the simulation with brine shows a larger algal bloom at both sites. In addition, the peak of the bloom is earlier at the LSC site under the thinner ice cover. These results give support to the suggestion that loss of habitat at the ice base through melting causes the termination of the algal bloom [Lizotte, 2003].

The growth and loss of ice algae over the bloom is displayed in Figure 8. In the

first half of the period, algal growth is larger than algal melt loss, consistent with the gain of biomass seen in Figure 7c and 7d. The peak algal growth is more pronounced at the HSC site around day 161. Growth at the LSC site is likely diminished at this time because the algal melt loss begins earlier at that site, resulting in less algae available to grow in the ice. The decline of the bloom begins in early to mid june (day 160 to 165), marked at both sites by the loss overtaking the growth. This timing is again consistent with the findings of Lavoie et al. [2005]. Therefore it seems that despite heightened light availability at the end of the study period, melting at the ice base dominates and the bloom ends.

It is important, when comparing simulated values of biomass with observations, to consider spatial variability. The model assumes the simulated algal bloom occurs in a fixed location in the ice, but the ice core position varied at both sites (chosen where snow thickness was 10 or 20 cm). Since there was blowing snow over the study period, a core sample under a 10 or 20 cm snow cover might have previously been under a much different snow thickness during sampling 3 days earlier. Thus, biomass collected might not always reflect levels expected for the simulated snow cover. Taking into account the discrepancies between simulated and observed values, results given in the previous section show that the model simulates the algal blooms reasonably well at the HSC and LSC sites. However there are still aspects of the model that can be improved - see the next section, 4.4.

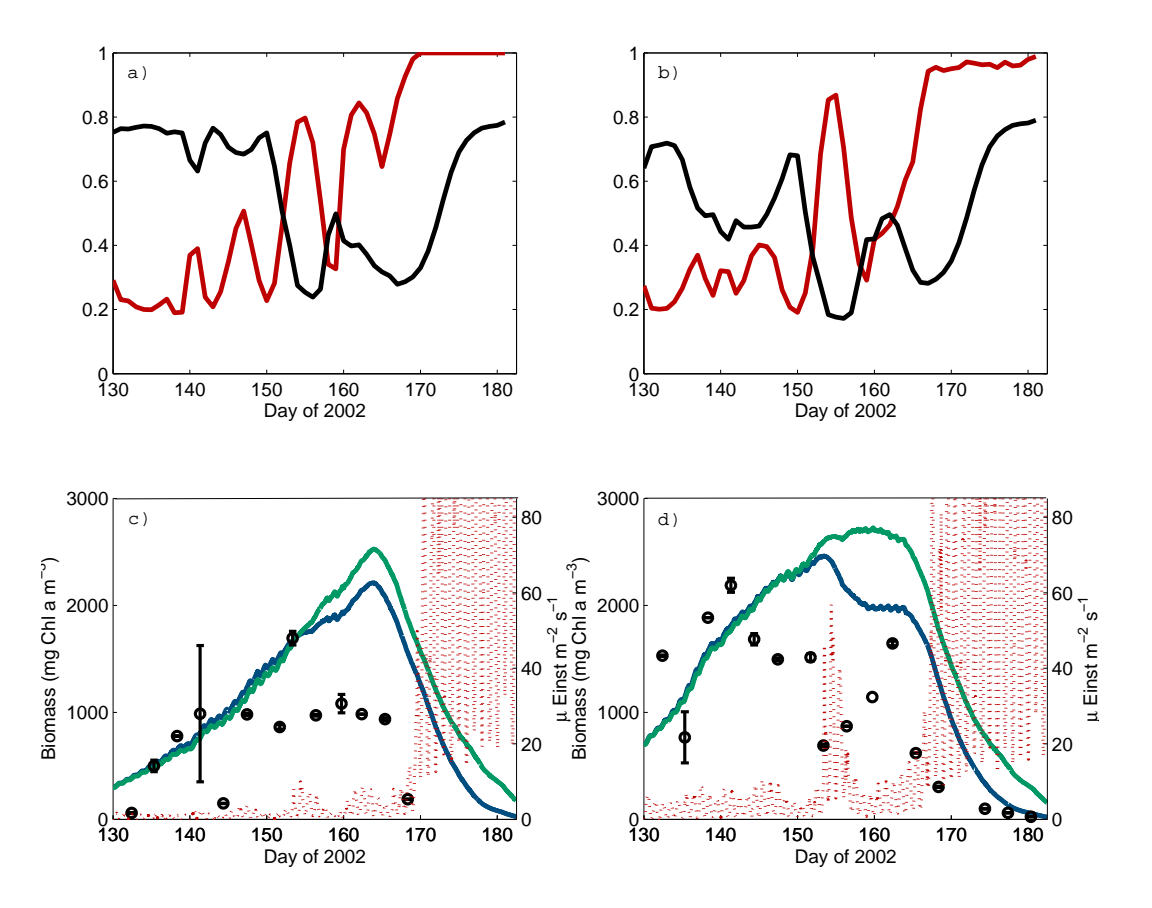


Figure 7: Model results versus observations for the HSC (left panel) and LSC sites (right panel). In (a) and (b), nutrient (black line,  $N_{lim}$ ) and light (red line,  $L_{lim}$ ) limitation functions; in (c) and (d), time series of observed (black circles) and simulated bottom ice biomasses, with (green line) and without (blue line) brine, and modeled PAR available at the top of the bottom ice layer. The vertical bars onn ice algal biomass observations represent the standard deviation over three ice cores.

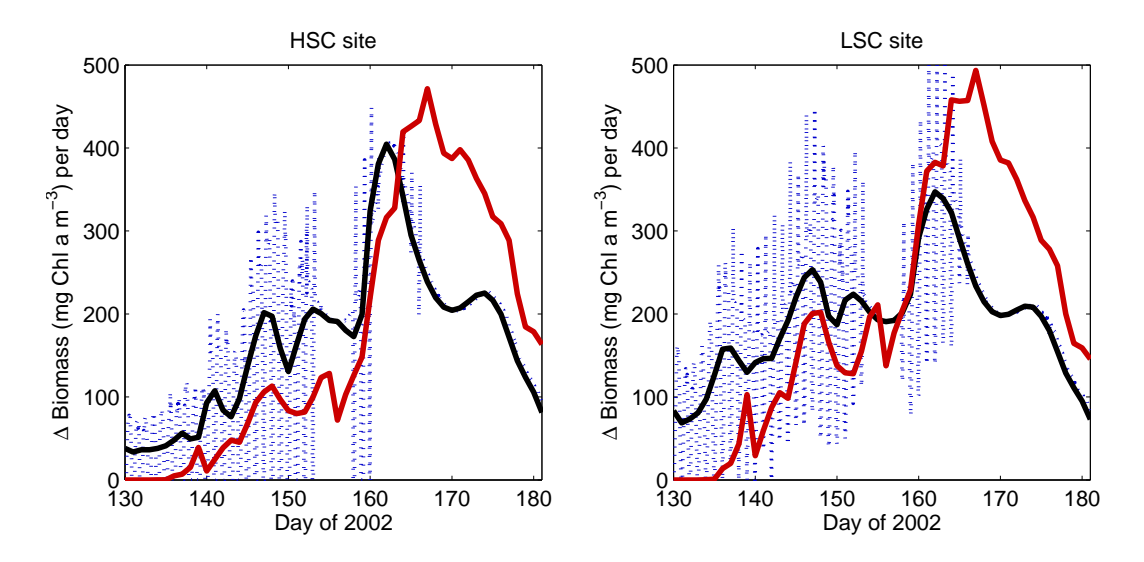


Figure 8: Simulated biomass growth (quarter hourly, dotted blue; daily mean, black line) and biomass loss through melt (red line) for the brine model run at the HSC (left panel) and LSC sites (right panel).

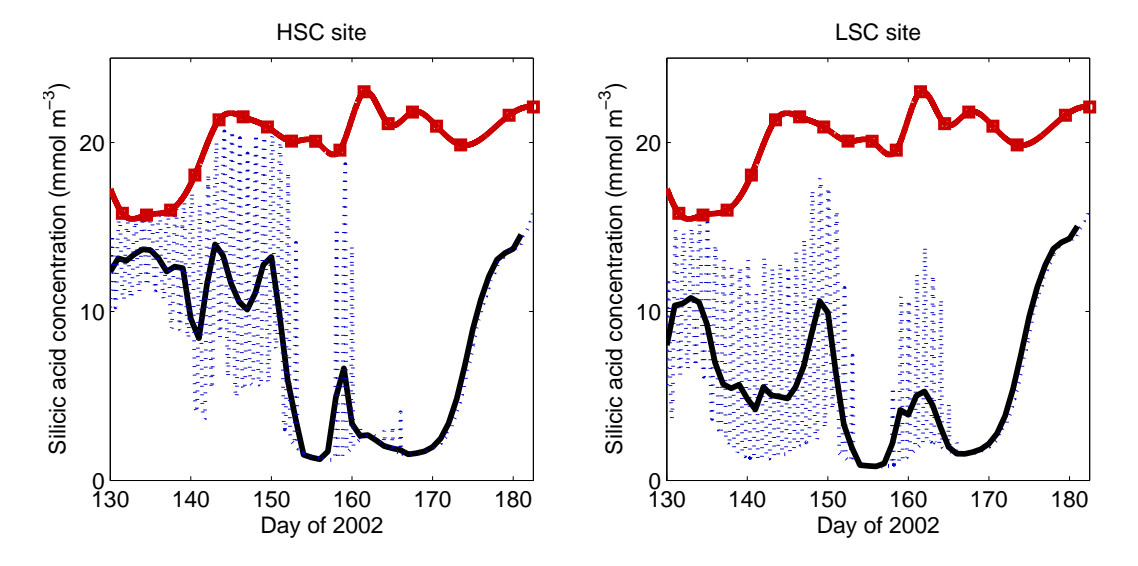


Figure 9: Simulated (solid red line) and observed (red squares) silicic acid concentration 2.5 m below the ice, and simulated silicic acid concentration in the bottom ice layer (quarter hourly, dotted blue; daily mean, black line) for the brine model run at the HSC(left panel) and LSC sites (right panel).

## 4.4 Sensitivity Analysis

### 4.4.1 Brine flushing

The effect of brine dynamics in the sea ice is not included in the model. Brine flushing, included in a brine dynamics model, is one process that becomes important during the spring melt. During this period, as brine pockets enlarge and become interconnected, a permeability threshold is reached and surface meltwater flows through the ice matrix [Vancoppenolle et al., 2007]. With meltwater moving through the brine channels, it is difficult for ice algae to maintain their position in the ice and algal loss from the ice increases [Krembs et al., 2001. At both sites, snow is melting during the study period and flushing of nutrients and algae should be taken into account. It may be especially important at the HSC site, where the thicker snow cover and its larger source of meltwater could favour more flushing as the snow melts. To study the sensitivity of the biomass bloom to flushing, we add a simple loss term proportional to the surface melt rate to the algae model, that is effective when the permeability threshold is reached. Following Vancoppenolle et al. [2007], the permeability threshold occurs when the brine volume e reaches 5%. In field experiments, once the brine network is permeable, the flushing of meltwater through the ice is almost immediate [Vancoppenolle et al., 2007]. I thus compute the new algal loss using the simultaneous surface melt at that time. The brine volume is given by:

$$e = -\mu_e \frac{S}{T}$$

where  $\mu_e = 0.054^{\circ}$ C psu<sup>-1</sup>, and S is salinity. After adding this new loss term, modeled biomass is in better agreement with observations (see Figure 10).

Drops in the simulated biomass levels are now seen between day 151 and 154 and day 160 and 163 at the HSC site, and between day 151 and 154 at the LSC site. These time periods correspond to periods with a significant decrease in observed snow thickness, and are likely times when algae are flushed out. Note that the variability in the observations is larger than in the model, suggesting that the flushing may have a larger effect than simulated.

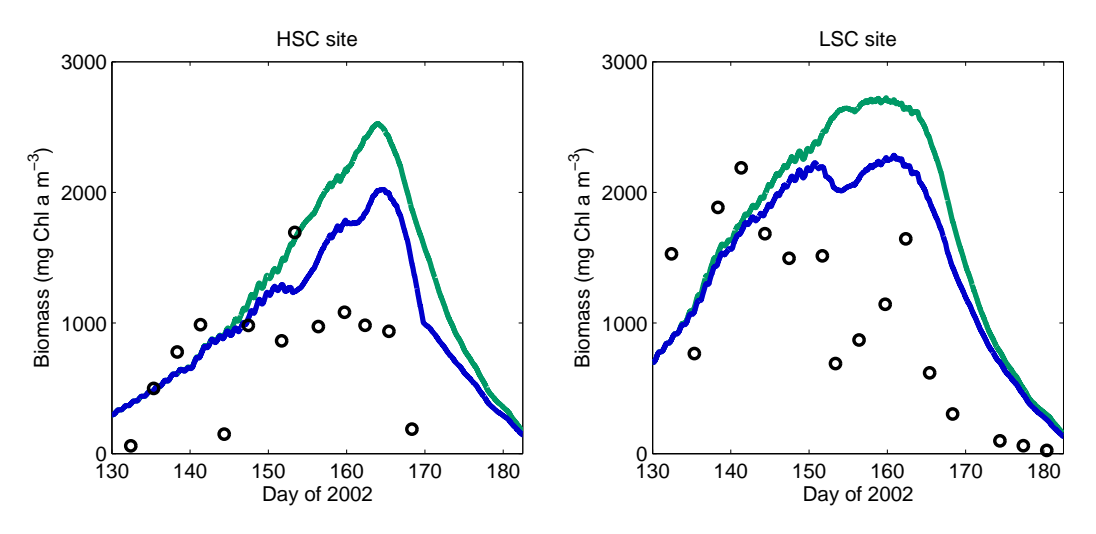


Figure 10: Observed (black circles) and simulated biomasses at HSC (left panel) and LSC sites (right panel): the control run (green line, same as simulation with brine in Figure 7) is compared to biomasses obtained using a primitive flushing term (blue line).

### 4.4.2 Freshwater lens

The decline of the simulated bloom occurs when algae lost from melt is larger than algal growth. The simulated rate at which the algae declines is slower than the observed decline (Figure 7c and 7d). A likely explanation for the discrepancy is the presence of a freshwater layer (e.g. 0.25 - 0.5 m thick, from Gosselin et al. [1990]) produced under the ice that is not described by the model. Created from the snow and ice melting, this freshwater lens restricts the nutrients from entering the ice and consequently slows growth. The first way by which it does this is through increased stratification below the ice,

which reduces the upward mixing of nutrients [Lavoie et al., 2005]. Second, the friction velocity becomes smaller, thereby increasing the viscous sublayer thickness and reducing diffusion of nutrients into the ice [Lavoie et al., 2005]. To accurately reproduce this effect, the relationship between the meltwater lens and friction velocity must be specified. If known, a parameterization can be added to the model, allowing snow and ice melt to influence the friction velocity. However, this process is poorly understood, and in the following I introduce a simple restriction to the model that halves the nutrient flux into the ice after the bloom begins its decline in early june. While this specific nutrient reduction cannot be justified, it gives an indication of how the melt lens could influence the end of the bloom. Including this condition does result in a more rapid bloom decline, although the effect is less pronounced in the final days of the observed bloom (see Figure 11). A more sophisticated handling of the meltwater lens that includes an increasingly limited nutrient flux may better describe the bloom end. Although these model additions are primitive, they show evidence that properly handling brine flushing and the meltwater lens in the model will likely improve the accuracy of the simulated algal blooms. These effects will be included in the model when it is coupled to Vancoppenolle et al. |2007| (see future work in the conclusion section).

## 4.4.3 Self shading

An improvement of this model over previous approaches is that it allows for algal growth through all ice layers. With  $w_{max}$  defined as 1.7 cm d<sup>-1</sup> [Krembs et al., 2001], the ice always grows slowly enough that algae can maintain their position in the bottom ice layer. Although this is where the overwhelming majority of ice algae are found in Arctic coastal ice blooms, it is possible that through the interconnection of brine channels, algae are able to grow upward

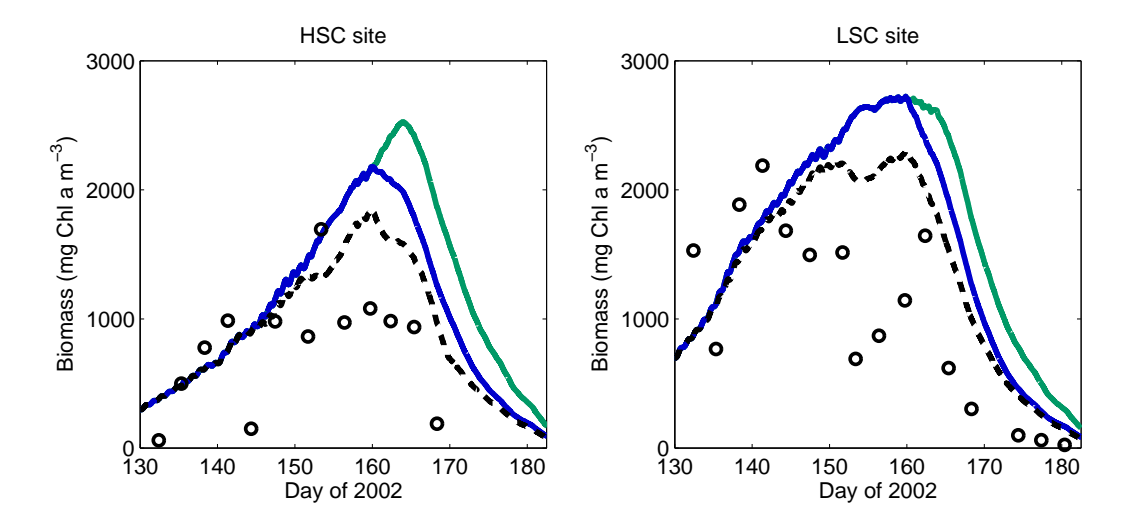


Figure 11: Observed (black circles) and simulated biomasses at HSC (left panel) and LSC sites (right panel): the control run (green line, same as simulation with brine in Figure 7) is compared to biomasses obtained using a melt lens parameterization (blue line), and using a melt lens parameterization combined with a flushing term (dotted black line).

into the ice [Horner et al., 1992]. Indeed, observations of chl a concentrations in the Resolute area are more vertically extensive in later spring until the bloom decline [Cota et al., 1991].

While algae deeper in the ice interior would receive more light, nutrients may be less accessible. In addition, algae growing at the base of the ice will be partly shaded from algae higher in the ice. To investigate how migration of algae effect the bloom dynamics, I choose  $w_{max} = 0.5$  cm day<sup>-1</sup>, which lets a fraction of the algae grow into the ice. The results (see Figure 12a) show a significant decrease in the peak biomass level reached at both sites. The total amount of biomass advected above the bottom layer is not significant (Figure 12b), but nonetheless reduces the light available to the algae in the layers beneath and slows growth. Overall, allowing some algae to grow more extensively in the ice gives a better match to observations, suggesting that a lower value of  $w_{max}$  would be in order.

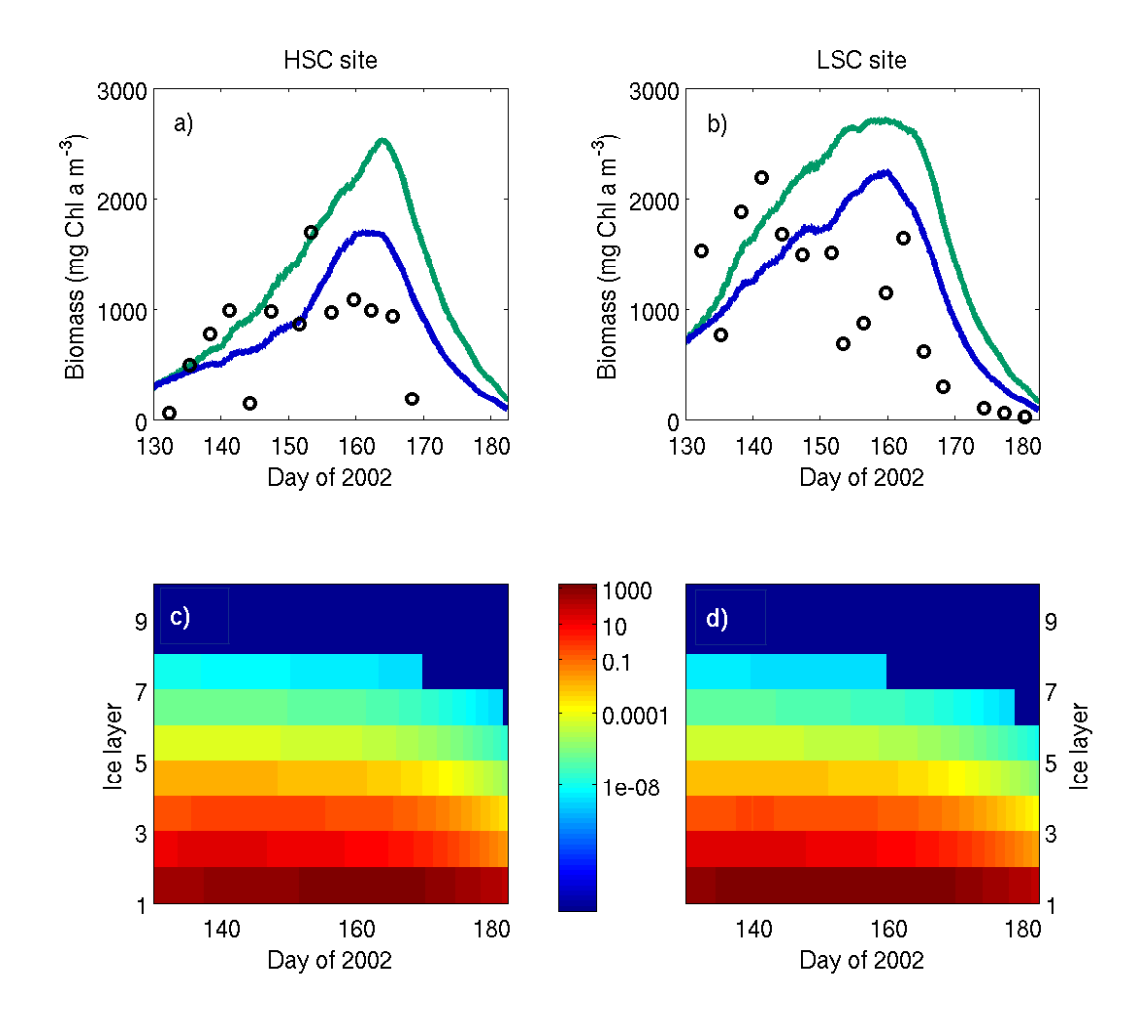


Figure 12: In (a) (HSC site) and (b) (LSC site), observed (black circles) and simulated biomasses: the control run (green line, same as simulation with brine in Figure 7) is compared to a simulation where algae are allowed to be advected into higher layers (blue line). In (c) (HSC site) and (d) (LSC site), time series of biomass in the bottom 10 ice layers, in mg chl a m<sup>-3</sup>.

### 4.4.4 Oceanic heat flux

The majority of the ice melt occurs at the ice base during the study period, when there is still an insulating snow cover. Since algal loss is dependent on the ice melt rate, the flux of heat from the ocean is an important controlling factor on the bloom. Here I look at the sensitivity of the algal bloom to 4 different treatments of the oceanic heat flux.

The oceanic heat flux  $F_{ocn}$  is calculated as follows:

$$F_{ocn} = \rho_o c_{po} C_{oi} u_\tau (T - T_f) = \rho_o c_{po} C_{oi} u_\tau (T + \mu_e S))$$

where  $\rho_o$ ,  $c_{po}$ , and T are the mixed layer density, heat capacity and temperature,  $C_{oi}$  is the ocean-ice sensible heat transfer coefficient, S is the ice base salinity, and  $T_f$  is the salinity dependent freezing point temperature. The heat flux used in this model control run was kept as in  $Huwald\ et\ al.$  [2005], with  $\rho_o=1025\ \mathrm{kg\ m^{-3}},\ c_{po}=3990\ \mathrm{J\ kg^{-1}\ K^{-1}},\ C_{oi}=0.001,\ \mathrm{and}\ u_{\tau}=0.05\ \mathrm{m}\ \mathrm{s^{-1}}.$  Values for T were taken from under-ice data. The parameterization of oceanic heat flux of  $Lavoie\ et\ al.$  [2005] uses in situ under-ice data for  $\rho_o$ , and T, and  $C_{oi}$  is calculated after  $McPhee\ [1992]$ . Their value of  $u_{\tau}$  varies based on the neap-spring tidal cycle in the area. Using tidal data,  $u_{\tau}$  was fitted to a sinuisoidal curve with a period of 14 days. Using this parameterization, the range of values for  $u_{\tau}$  falls between  $(8\times10^{-3}\ \mathrm{m\ s^{-1}})$  for neap tides and  $(4\times10^{-3}\ \mathrm{m\ s^{-1}})$  for spring tides.

While both use slightly different formulations, the resulting  $F_{ocn}$  are very similar (Figure 13). In the following, the heat flux formulation by  $Huwald\ et\ al.$  [2006] is called CTR, and that of  $Lavoie\ et\ al.$  [2005] is referred to as Ocean Flux 2. These are further compared with results from two other fluxes. Ocean

Flux 3 is obtained by taking the CTR flux and setting  $u_{\tau} = 0.06 \text{ m s}^{-1}$  to give a slightly larger flux than the control. Ocean Flux 4 also makes a seemingly small change, of reducing  $\mu_e$  by 0.001 to 0.054 in the *Lavoie et al.* [2005] calculation. A comparison of the four daily mean oceanic heat fluxes shows the first three fluxes to be very similar to each other, with Ocean Flux 4 being slightly lower overall (see Figure 13).

Of the model results obtained using each of the fluxes, three out of four runs

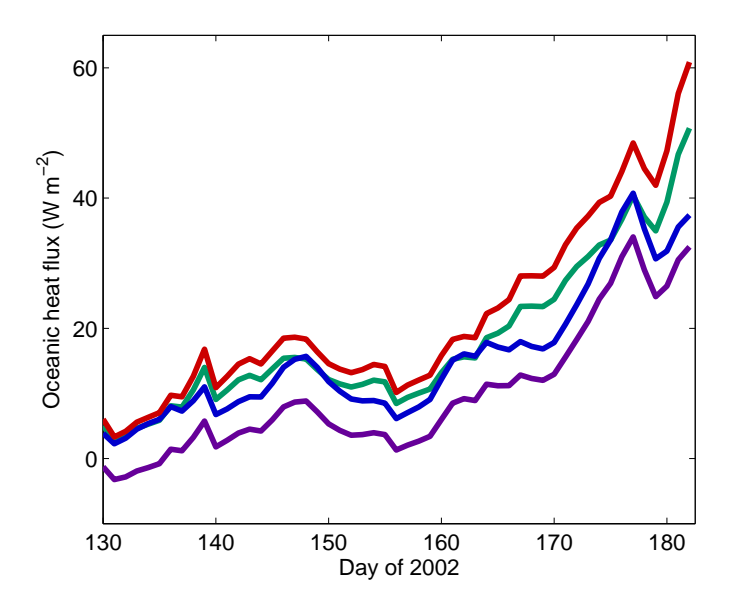


Figure 13: a) The oceanic heat flux used in the control run (green line), and three other simulated oceanic heat fluxes used for comparison: flux 2, that of [Lavoie et al., 2005] (blue line), flux 3, control flux with  $u_{\tau}$  increased by 0.01 m s<sup>-1</sup> (red line), and flux 4, [Lavoie et al., 2005] with  $\mu_e$  reduced by 0.001 (purple line).

have good agreement with ice thickness observations (Figure 14a). However even a small change to  $\mu_e$  (Ocean Flux 4) results in an ocean heat flux that is too low and does not effectively capture the observed melt. The effect of the different ice thickness evolutions on the algal bloom is presented in Figure 14b. While each of the first three fluxes give very similar ice thicknesses, the difference between peak biomasses in each of the runs is fairly significant. For instance CTR flux and Ocean Flux 2 are very similar, the peak biomass at the LSC site rises from around 2700 mg chla m<sup>-3</sup> in the control run to about 3500 mg chla m<sup>-3</sup> using Ocean Flux 2. Thus, with similar ocean fluxes and ice thicknesses giving significantly different bloom peaks, it seems that the algal bloom is very sensitive to the oceanic heat flux and its effect on algal melt loss at the ice base. While interesting, this is of concern since the exact details of oceanic heat flux, through its small scale processes, is difficult to capture even in current ice-ocean models with high vertical resolution.

### 4.4.5 Viscous sublayer thickness

The viscous sublayer thickness  $h_{\nu}$  affects the oceanic heat flux (inversely related) as well as the nutrient flux to the ice base. With the oceanic heat flux contributing to algal loss through melting and the nutrient flux contributing to algal growth, the two fluxes work in opposing ways. For example by decreasing the thickness of the viscous sublayer, the nutrient flux from the water column is enhanced, aiding algal growth. On the other hand the flux of warmer ocean water to the ice base is also increased, resulting in more melting and loss of algae. In *Lavoie et al.* [2005], a sensitivity analysis of the viscous sublayer thickness showed the overall impact on the algae, with the oceanic heat flux dominating the nutrient flux. I perform a similar sensitivity test on the viscous sublayer thickness, but concentrating on its effect on the nutrient flux alone.

The parameterization of  $u_{\tau}$  based on the tidal cycle, described in section 4.4.4, is used in this model when calculating the nutrient flux. Because of the relationship between  $u_{\tau}$  and  $h_{\nu}$  (see equation 13),  $h_{\nu}$  also follows a sine curve. The first test is to set  $h_{\nu}$  to a constant equal to the mean value over the monthly tidal cycle. This does not yield a significant change in biomass (see

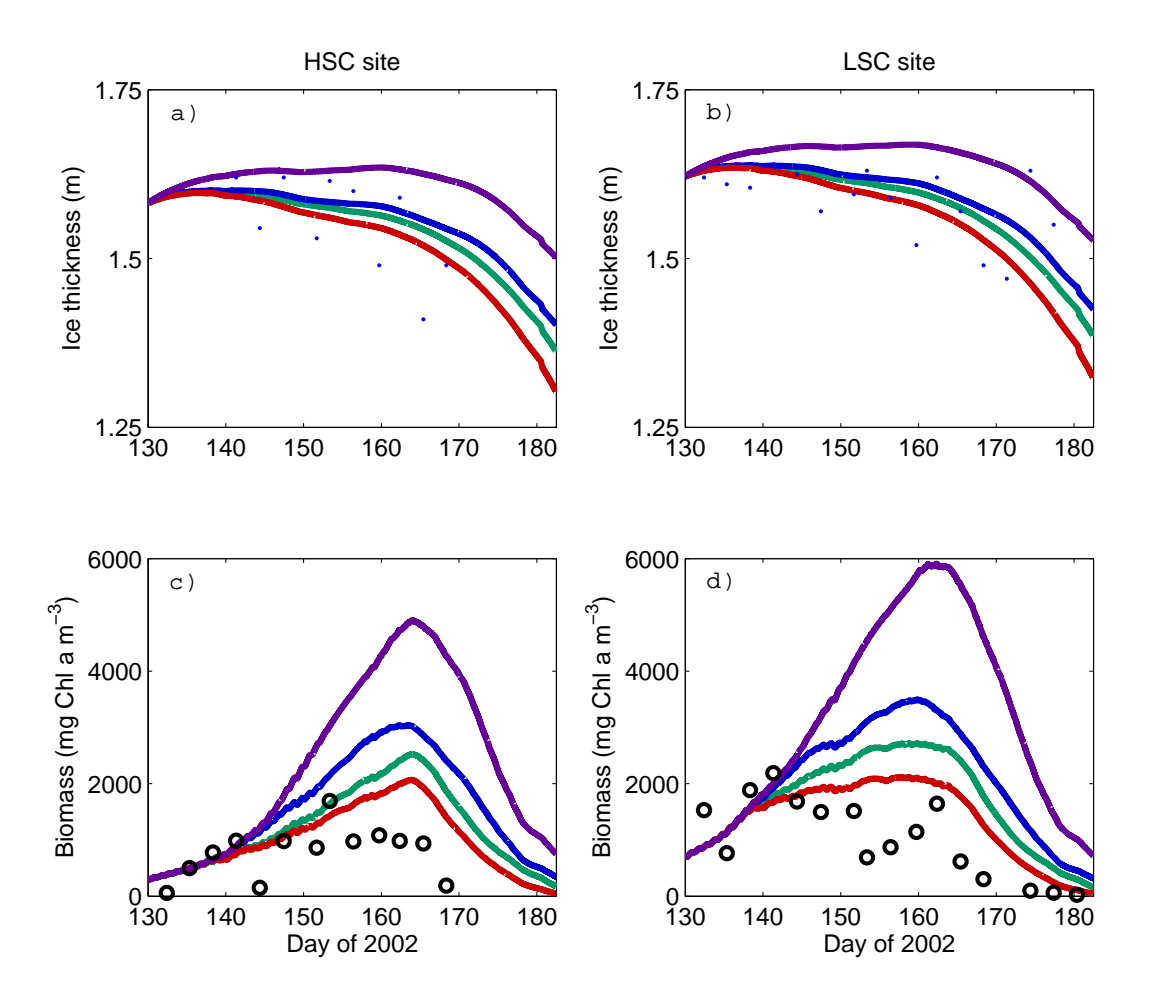


Figure 14: In (a) (HSC site) and (b) (LSC site), observed (blue dots) and simulated ice thicknesses corresponding to the control run (green line), flux 2 (blue line), flux 3 (red line), and flux 4 (purple line) (see Figure 13). In (c) (HSC site) and (d) (LSC site), observed (black circles) and simulated biomasses: the control run (green line, same as simulation with brine in Figure 7) is compared to biomasses corresponding to flux 2 (blue line), flux 3 (red line), and flux 4 (purple line).

Figure 15). I also run two simulations with  $h_{\nu}$  again following a sinusoidal curve, but with the original mean value of 0.3 mm raised and lowered by 0.1 mm. This alteration makes a notable difference, especially the case in which  $h_{\nu}$  is smaller (Figure 15). The results of Lavoie et al. [2005] show that with a reduced viscous sublayer thickness, algal loss associated with the enhanced oceanic heat flux was greater than the algae gained from an enhanced nutrient flux. Considering the excess algae gained from the higher nutrient flux seen in Figure 15, a corresponding change to the oceanic heat flux must have a large impact to eclipse the nutrient flux. This provides further support that the oceanic heat flux could be an important factor in algal biomass variability.

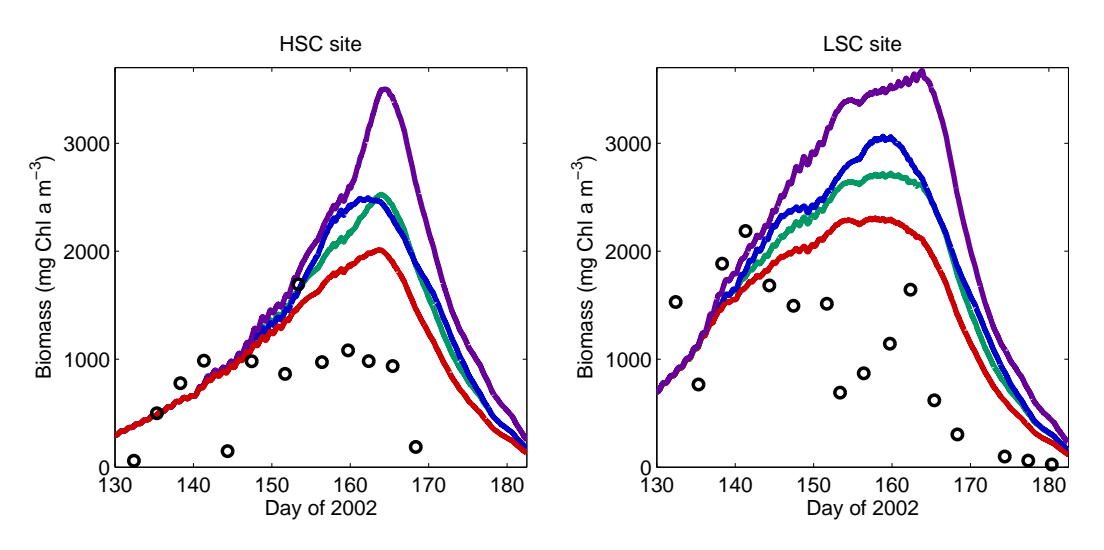


Figure 15: Observed (black circles) and simulated biomasses at HSC (left panel) and LSC sites (right panel): the control run (green line, same as simulation with brine in Figure 7) is compared to biomasses obtained using a constant  $h_{\nu} = 0.3$  mm (blue line), and an altered mean  $h_{\nu}$  of 0.2 mm (purple line) and 0.4 mm (red line).

### 4.4.6 Grazing

Large protozoa, metazoa, amphipods and copepods can all potentially consume ice algae, and there are many uncertainties in how to quantify this loss. How it varies over the algal bloom is also not well known. It is possible that during

the bloom decline, brine channel enlargement allows larger grazers to access the algae in the ice, resulting in increased grazing later in the bloom [Krembs et al., 2000]. Since grazing G is simply fixed to be 10% of the growth rate in this model, it is worthwhile to test the importance of this term. Results of the sensitivity test show that changing the grazing rate to 15% or 6.7% does not have a significant impact on the ice algal bloom (Figure 16). Increasing the amount of grazing during the second half of the bloom may improve the simulations resemblances to observations, but not substantially.

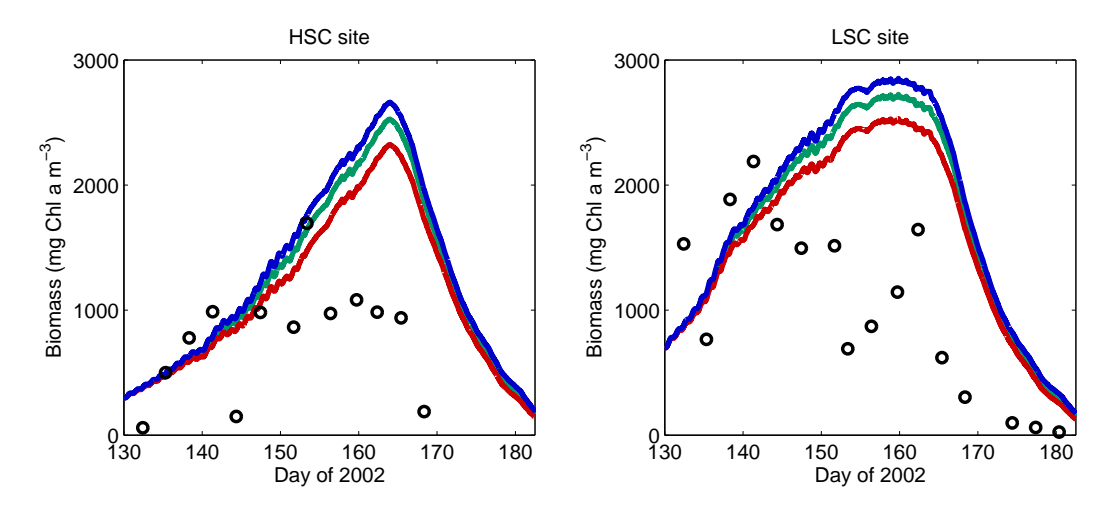


Figure 16: Observed (black circles) and simulated biomasses at HSC (left panel) and LSC sites (right panel): the control run (green line, same as simulation with brine in Figure 7) is compared to biomasses obtained using a grazing rate of 6.7% (blue line), and 15% (red line).

### 4.4.7 Biomass initial condition

The governing equations of ice algae and nutrients (see equations 18 and 19) are advection equations which require a boundary condition and initial condition to be well posed. The initial values are set from observations at the sites. Since there are uncertainties in the observations, there is a range of reasonable choices to use. In the control run, the initial value for biomass was chosen to be 300 mg chla m<sup>-3</sup> at the HSC site and 700 mg chla m<sup>-3</sup> at the LSC site

based on observations. Running the model with initial conditions of 150 and 500 mg chla  $m^{-3}$  for the HSC site and 1000 and 1500 mg chla  $m^{-3}$  for the LSC site gives practically the same results, suggesting the system is relatively stable to the initial conditions (Figure 17).

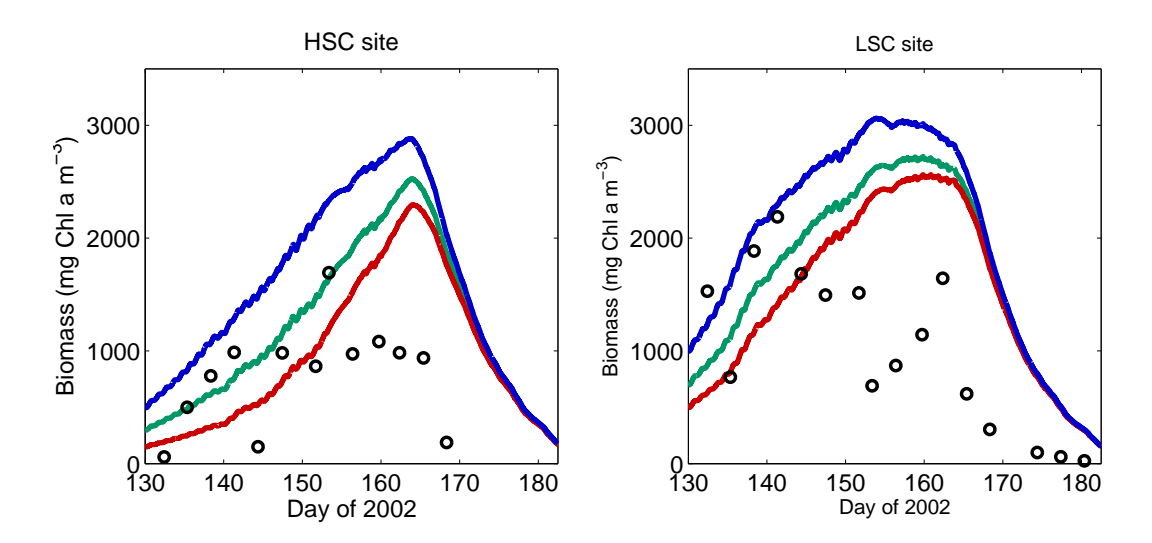


Figure 17: Observed (black circles) and simulated biomasses: the control run (green line, same as simulation with brine in Figure 7) is compared to biomasses obtained with an initial concentration of 150 (red line) and 500 mg chla m $^{-3}$  (blue line) at the HSC site (left panel), and with an initial concentration of 500 (red line) and 1000 mg chla m $^{-3}$  (blue line) at the LSC site (right panel).

# 5 Conclusion

I have introduced a new snow-ice-algae-nutrient column model, developed by coupling the ice algae-nutrient model of *Lavoie et al.* [2005] with the thermodynamic sigma-coordinate sea ice model of *Huwald et al.* [2005]. Model results were compared to observations made in Resolute Passage during spring 2002.

Results show that ice thickness has a large impact on algal biomass content at the ice base. Ice melt rate determines the amount of algae lost to the water column, through a direct impact on the ice algae habitat as well as through flushing and its effect on nutrient availability. In a simulation with brine not included, ice melt was higher and biomass was lower and declined earlier. Although more light was available for algal growth under the thinner ice cover, the ice melt rate had a larger impact on the fate of the bloom. This finding gives support to the suggestion made in other ice algal studies that the basal ice melt rate is the trigger for the algal bloom decline (e.g. Legendre et al. [1991]; Lizotte [2003]).

Because ice melt is so important to how the algal bloom develops, I introduced primitive parameterizations of brine flushing and melt water at the ice base. A closer match to observations using these parameterizations suggests that these mechanisms enhance the decline of the bloom. Therefore in addition to ice melt rate, it seems ice structure is also an important controlling factor of the algal bloom, in agreement with past studies (e.g. Gosselin et al. [1986]; Krembs et al. [2001]).

Snow cover is also a dominant factor in controlling algal bloom dynamics. Early in the bloom, the snow thickness is the harshest attenuator of light, thereby restricting algal growth. Through its influence on ice melt rate, a disappearing snow cover also plays an important role in the bloom decline. In addition, a thicker snow cover provides more freshwater during melting, contributing to the flushing and melt water lens effects during the bloom decline. These findings support past ice algae studies pinpointing snow cover as a dominant factor controlling bloom dynamics (e.g. Lavoie et al. [2005]; Cota and Smith [1991]; Welch and Bergmann [1989]).

The ice algae were found to be light limited at the beginning of the bloom, transitioning to a nutrient limitation by the bloom end. However, there were difficulties in matching simulated and observed under-ice PAR. Attaining the correct combination of light attenuation and extinction coefficients ( $\kappa_s$ ,  $\kappa_i$ ,  $i_0$ ), while accurately modeling the ice thickness evolution, is not a straightforward task. Both findings in the literature and results presented here suggest that with changing snow and ice conditions over the melt season,  $\kappa_s$  and  $\kappa_i$  should decrease over time, reducing light attenuation with increased melting. As well, it is possible  $i_0$  should increase as the melt season progresses, allowing more light to penetrate the surface layer. Especially in the case of  $i_0$  for snow, the choices for these parameters are not well known. Similar differences between simulated and observed under-ice PAR are found in Lavoie et al. [2005]. In order to effectively simulate ice algae at the ice base, this area requires further study.

Ice algae also seem to be strongly impacted by changing ocean conditions. Small changes to the oceanic heat flux, through its effect on basal ice melt, yield significant changes in biomass levels. The strong sensitivity to this parameterization is of concern, since the small scale features such as the melt water lens and stratification are not properly resolved in current high resolution ice-ocean models.

A new result of this multi-layer thermodynamic model, with its ability to model algae in all layers within the ice, is the effect of self shading. Allowing a small amount of ice algae to grow into the interior of the ice causes algae in the platelet layer at the ice base to receive less light and grow more slowly. The overall response of the biomass gave a better match to observations, suggesting this is a potentially important factor to include in a model.

Given the fragile balance of ideal nutrient, light and substrate conditions at the ice base, it is no surprise that the algae are so strongly influenced by ice melt, water column stratification and other physical conditions. While this thesis introduced a snow-ice-algae-nutrient model that is more physically sound than past model studies, it also revealed the need for improvements. Results suggest that being able to accurately simulate physical conditions at the ice base is essential before ice algae can be reliably modeled.

The next development of this model will handle the presence of algae in the ice interior more realistically. To this end, I will include two more sources of nutrients: through brine drainage from higher in the ice, and in situ regeneration of biogenic materials. Processes such as brine drainage will be represented in the model when it is coupled to the brine dynamics model of *Vancoppenolle et al.* [2007]. In addition to brine drainage, a more sophisticated parameterization of brine flushing will be added, enabling the model to capture the loss of algae during melt more effectively.

#### 6 References

Aagaard, K., and E.C. Carmack (1989), The role of sea ice and other fresh water in the Arctic circulation, *J. Geophys. Res.*, 94, 14485-14498.

Ackley, S.F., K.R. Buck, and S. Taguchi (1979), Standing crop of algae in the sea ice of the Weddell Sea region, *Deep-Sea Res.* 26A, 269-281.

Arnell, N.W. (2005), Implications of climate change for freshwater inflows to the Arctic Ocean, J. Geophys. Res., 110, D07105, doi:10.1029/2004JD005348.

Arrigo, K.R., J.N. Kremer, and C.W. Sullivan (1993), A simulated Antarctic fast-ice ecosystem, *J. Geophys. Res.*, 98(C4), 6929-6946.

Arrigo, K.R. and C.W. Sullivan (1994), A high resolution bio-optical model of microalgal growth: Tests using sea ice algal community time series data, Limnol. Oceanogr., 39, 609631.

Belanger, S., H. Xie, N. Krotkov, P. Larouche, W.F. Vincent, and M. Babin (2006), Photomineralization of terrigenous dissolved organic matter in Arctic coastal waters from 1979 to 2003: Interannual variability and implications of climate change, *Global Biogeochem. Cycles*, 20, GB4005, doi:10.1029/2006GB002708.

Benner, R., B. Benitez-Nelson, K. Kaiser, and R.M.W. Amon (2004), Export of young terrigenous dissolved organic carbon from rivers to the Arctic Ocean, *Geophys. Res. Lett.* 31, L05305, doi:10.1029/2003GL019251.

Bitz, C.M., and W.H. Lipscomb (1999), An energy-conserving thermodynamic model of sea ice, *J. Geophys. Res.*, 104, 15669-15677.

Carmack, E.C., R.W. Macdonald, and S.E. Jasper (2004), Pelagic phytoplankton productivity on Canadian shelf of the Beaufort Sea, *Mar. Ecol. Prog. Ser.* 277, 3750.

Cavalieri, D.J., C.L. Parkinson, and K.Y. Vinnikov (2003), Thirty-year satellite record reveals contrasting Arctic and Antarctic decadal sea ice variability, *Geophys. Res. Lett.* 30(18), 1970, doi:10.1029/2003GL018031.

Christensen, T.R., and P. Cox (1995), Response of methane emissions from arctic tundra to climatic change: results from a model simulation, *Tellus B47*,

301309.

Cota, G.F., and E.P.W. Horne (1989), Physical control of Arctic ice algal production, *Mar. Ecol. Prog. Ser.*, 52, 111-121.

Cota, G.F., and R.E.H. Smith (1991), Ecology of bottom ice algae: II. Dynamics, distributions and productivity, *J. Mar. Syst.*, 2, 279-295.

Cota, G.F., S.J. Prinsenberg, E.B. Bennett, J.W. Loder, M.R. Lewis, J.L. Anning, N.H.F. Watson (1987), Nutrient fluxes during extended blooms of Arctic ice algae, *J. Geophys. Res.* 92, 1951-1962.

Cota, G.F., J.L. Anning, L.R. Harris, W.G. Harrison, and R.E.H. Smith (1990), The impact of ice algae on inorganic nutrients in seawater and sea ice in Barrow Strait, NWT, Canada during spring, *Can. J. Fish. Aquat. Sci.*, 47, 1402-1415.

Cota, G.F., L. Legendre, M. Goesselin, and R.G. Ingram (1991), Ecology of bottom ice algae: I. Environmental controls and variability, *J. Mar. Syst.*, 2, 257-277.

Eppley, R.W. (1972), Temperature and phytoplankton growth in the sea, *Fish. Bull.*, 70, 1063-1085.

Fioletoc, V.E., M.G. Kimlin, N. Krotkov, L.J.B. McArthur, J.B. Kerr, D.I. Wardle, J.R. Herman, R. Meltzer, T.W. Mathews, and J. Kaurola (2004), UV index climatology over the United States and Canada from ground-based and satellite estimates, *J. Geophys. Res.*, 109(D22), D22308, doi:10.1029/2004JD004820.

Flato, G.M., and R.D. Brown (1996), Variability and climate sensitivity of landfast Arctic sea ice, *J. Geophys. Res.*, 101 (C10), 26767-26777.

Fortier, M., L. Fortier, C. Michel, and L. Legendre (2002), Climatic and biological forcing of the vertical flux of biogenic particles under seasonal Arctic sea ice, *Mar. Ecol. Prog. Ser.* 225, 116.

Gobeil, C., B. Sundby, R.W. Macdonald, and J.N. Smith (2001), Recent change in organic carbon flux to Arctic Ocean deep basins: Evidence from acid volatile silfide, manganese and rhenium discord in sediments, *Geophys. Res. Lett.* 28(9): 1743-1746.

Gosselin, M., L. Legendre, S. Demers, and R.G. Ingram (1985), Responses of sea-ice microalgae to climatic and fortnightly tidal energy inputs (Manitounuk Sound, Hudson Bay), Can. J. Fish. Aquat. Sci., 42, 999-1006.

Gosselin, M., L. Legendre, J.-C. Therriault, S. Demers, M. Rochet (1986), Physical control of the horizontal patchiness of sea-ice microalgae, *Mar. Ecol. Prog. Ser.* 29, 289298.

Gosselin, M., L. Legendre, J.-C. Therriault, and S. Demers (1990), Light and nutrient limitation of sea-ice microalgae (Hudson Bay, Canadian Arctic), *J. Phycol.*, 26, 220-232.

Gosselin, M., M. Levasseur, P.A. Wheeler, R.A. Horner, B.C. Booth (1997), New measurements of phytoplankton and ice algal production in the Arctic Ocean, *Deep-Sea Res.* 44, 1623-1644.

Gradinger, R. (1996), Occurrence of an algal bloom under Arctic pack ice, Mar. Ecol. Prog. Ser. 131, 301305.

Gradinger, R. (1999), Vertical fine structure of the biomass and composition of algal communities in Arctic pack ice, *Mar. Biol.* 133, 745754.

Gradinger R., and Q. Zhang (1997), Vertical distribution of bacteria in sea ice from the Barents and Laptev Seas, *Polar Biol* 17, 448-454.

Grenfell, T.C., and G.A. Maykut (1977), The optical properties of ice and snow in the Arctic basin, *J. Glaciol.*, 1880, 445-463.

Grigoriev, M.N., V. Rachold, H.-W. Hubberten, and L. Schirrmeister (2004), Organic carbon input to the Arctic Seas through coastal erosion, in *The organic carbon cycle in the Arctic Ocean*, edited by R. Stein and R.W. MacDonald, pp.41-45, Springer, Berlin.

Horner, R.A., S.F. Ackley, G.S. Dieckmann, B. Gulliksen, T. Hoshiai, L. Legendre, I.A. Melnikov, W.S. Reeburgh, M. Spindler and C.W. Sullivan (1992), Ecology of sea ice biota. 1. Habitat, terminology, and methodology, *Polar Biol.* 12, 417427.

Huwald, H., L.-B. Tremblay, and H. Blatter (2005), A multilayer sigma-coordinate thermodynamic sea ice model: Validation against Surface Heat Budget of the Arctic Ocean (SHEBA)/Sea Ice Model Intercomparison Project Part 2

(SIMIP2) data, J. Geophys. Res., 110, C05010, doi:10.1029/2004JC002328.

Johannessen, O.M., L. Bengtsson, M.W. Miles, S.I. Kuzmina, V.A. Semenov, G.V. Aledseev, A.P. Nagumyi, V.F. Zakharov, L.P. Bobylev, L.H. Pettersson, K. Hasselmann, and H.P. Cattle (2004), Arctic climate change: observed and modelled temperature and sea-ice variability, *Tellus* 56A, 328341.

Kirk, J.T.O. (Ed.) (1983), Light and Photosynthesis in Aquatic Ecosystems, 401 pp., Cambridge Univ. Press, New York.

Kowalik, Z., and A.Y. Proshutinsky (1994), The Arctic Ocean tides, in *The polar oceans and their role in shaping the global environment*, edited by O.M. Johannessen, R.D. Muench, and J.E. Overland, pp. 137-158, AGU, Washington.

Krembs, C., R. Gradinger, and M. Splinder (2000), Implications of brine channel geometry and surface area for the interaction of sympagic organisms in Arctic sea ice, *J. Exp. Mar. Biol. Ecol.*, 243, 55-80.

Krembs, C., T. Mock, and R. Gradinger (2001), A mesocosm study on physical-biological interactions in artificial Arctic sea ice, *Polar Biol.*, 24, 356-364.

Lavoie, D., K. Denman, and C. Michel (2005), Modeling ice algal growth and decline in a seasonally ice-covered region of the Arctic (Resolute Passage, Canadian Archipelago), *J. Geophys. Res.*, 110, C11009, doi: 10.1029/2005JC002922.

Lavoie, D., R.W. Macdonald, and K.L. Denman (2009), Primary productivity and export fluxes on the Canadian shelf of the Beaufort Sea: A modelling study, *J. Mar. Syst.*, 75, 17-32.

Legendre, L., M. Aota, K. Shirasawa, M.J. Martineau, and M. Ishikawa (1991), Crystallographic structure of sea ice along a salinity gradient and environmental control of microalgae in the brine cells, *J. Mar. Syst.*, 2, 347-357.

Legendre, L., S.F. Ackley, G.S. Dieckmann, B. Gulliksen, R. Horner, T. Hoshiai, I.A. Melnikov, W.S. Reeburgh, M. Spindler, and C.W. Sullivan (1992), Ecology of sea ice biota: 2. Global significance, *Polar Biol.*, 12, 429-444.

Leventer, A. (2003), Particulate flux from sea ice in polar waters, in *Sea Ice:* An Introduction to its Physics, Chemistry, Biology and Geology, edited by D.N.

Thomas and G.S. Dieckmann, pp. 303-332, Blackwell Sci., Malden, Mass.

Liebner, S., and D. Wagner (2006), Abundance, distribution and potential activity of methane oxidising bacteria in permafrost soils from the Lena Delta, Siberia, *Environ. Microbiol.*, 9, 107117.

Light, B., T.C. Grenfell, and D.K. Perovich (2008), Transmission and absorption of solar radiation by Arctic sea ice during the melt season, *J. Geophys. Res.*, 113, C03023, doi:10.1029/2006JC003977.

Lizotte, M.P. (2003), The microbiology of sea ice, in *Sea Ice: An Introduction to its Physics, Chemistry, Biology and Geology*, edited by D.N. Thomas and G.S. Dieckmann, pp. 184-210, Blackwell Sci., Malden, Mass.

Maykut, G.A. (1985), The ice environment, in *Sea Ice Biota*, edited by R.A. Horner, pp. 21-82, CRC Press, Boca Raton, Fla.

Meguro, H., K. Ito, and H. Fukushima (1967), Ice flora (bottom type): A mechanism of primary production in polar seas and the growth of diatoms in sea ice, *Arctic*, 20, 114-133.

Meiners, K., R. Gradinger, J. Fehling, G. Civitarese, and M. Spindler (2003), Vertical distribution of exopolymer particles in sea ice of the Fram Strait (Arctic) during autumn, *Mar. Ecol. Prog. Ser.*, 248, 113.

Michel, C., L. Legendre, R.G. Ingram, M. Gosselin, and M. Levasseur (1996), Carbon budget of sea-ice algae in spring: Evidence of a significant transfer to zooplankton grazers, *J. Geophys. Res.*, 101, 1834518360.

Nishi, Y., and S. Tabeta (2005), Analysis of the contribution of ice algae to the ice-covered ecosystem in Lake Saroma by means of a coupled ice ocean ecosystem model, *J. Mar. Syst.*, 55, 249–270.

Ohmura, A. (1984), Comparative energy balance study for Arctic tundra, sea surface glaciers and boreal forests, *J. Geophys. Res.*, 8, 221-228.

Parkinson, C.L., and W.M. Washington (1979), A large-scale numerical model of sea ice, *J. Geophys. Res.*, 84(C1), 311-337.

Platt, T., and V. Subba Rao (1975), The spectral distribution of light beneath

first-year sea ice in the Arctic Ocean, Limnol. Oceanogr., 20, 554-563.

Riebesell, U., I. Schloss, and V. Smetacek (1991), Aggregation of algae released from melting sea ice: implications for seeding and sedimentation, *Polar Biol.*, 11, 239248.

Sarthou, G., K.R. Timmermans, S. Blain, and P. Tréguer (2005), Growth physiology and fate of diatoms in the ocean: A review, J. Sea Res., 53, 25-42.

Smith, R.E.H., J. Anning, P. Clement, and G. Cota (1988), Abundance and production of ice algae in Resolute Passage, Canadian Arctic, *Mar. Ecol. Prog. Ser.*, 48, 251-263.

Smith, R.E.H., W.G. Harrison, L.R. Harris, and A.W. Herman (1990), Vertical fine structure of particulate matter and nutrients in sea ice of the high Arctic, Can. J. Fish. Aquat. Sci., 47, 1348-1355.

Spindler, M. (1990), A comparison of Arctic and Antarctic sea ice and the effects of different properties on sea ice biota, in *Geological history of the polar oceans: Arctic versus Antarctic*, edited by U. Bleil, J. Thiede, pp. 173-186, Kluwer Academic Publ, The Netherlands.

Tennekes, H., and J.L. Lumley (Eds.) (1972), A First Course in Turbulence, 300 pp., MIT Press, Cambridge, Mass.

Untersteiner, N. (1961), On the mass and heat budget of Arctic sea ice, Arch. Meteorol. Geophys. Bioklimatol., Ser. A, 12, 151-182.

Vancoppenolle, M., C.M. Bitz, and T. Fichefet (2007), Summer landfast sea ice desalination at Point Barrow, Alaska: Modeling and observations, *J. Geophys. Res.*, 112, C04022, doi:10.1029/2006JC003493.

Welch, H.E., and M.A. Bergmann (1989), Seasonal development of ice algae and its prediction from environmental factors near Resolute, N.W.T., Canada, Can. J. Fish. Aquat. Sci., 46, 1793–1804.

Weeks, W.F., and S.F. Ackley (1986), The growth, structure, and properties of sea ice, in *The geophysics of sea ice*, edited by N. Untersteiner, pp. 9-164, Plenum Press, New York.

Zeebe, R.E., H. Eicken, D.H. Robinson, D. Wolf-Gladrow, and G.S. Dieckmann (1996), Modeling the heating and melting of sea ice through light absorption by microalgae, J. Geophys. Res., 101 (C1), 1163-1181.

# Appendices

# A Internal melting

Modeling over the melt season, and allowing shortwave radiation to penetrate deeper into the interior snow and ice layers, requires a proper handling of internal melting. This issue was not important in  $Huwald\ et\ al.\ [2005]$ , which had values of  $i_0$  that resulted in most shortwave radiation being absorbed in the surface layer.

In the sea ice thermodynamic model, when the surface temperature (for snow or ice) rises above the freezing point, the temperature is brought down to the freezing point and the excess energy is used in melting. Considering the case with no snow, the temporal evolution of the ice surface during melting is determined by the net flux of energy at the surface:

$$\frac{\partial s_i}{\partial t} = \begin{cases} -(F_{net} + F_{cs})/(\rho_i L_f(S, T)), & \text{if } F_{net} + F_{cs} > 0\\ 0, & \text{if } F_{net} + F_{cs} = 0 \end{cases}$$

where variables are defined in section 2.1 and  $L_f(S,T)$  is the energy of melt given by

$$L_f(S,T) = c_{p0}(T_f - T) + L_{f0}\left(1 + \frac{\mu S}{T}\right)$$

The first term on the right hand side is the energy required to bring a unit mass of ice from temperature T to freezing temperature  $T_f$ , and the second term is the energy to melt the ice.

Because light penetrates more deeply during the spring melt, even with the

surface temperature being reset to the freezing point, it is possible to have above freezing temperatures simulated by the model in the internal layers as well. As a result it is important to keep track of excess energy in all layers and deal effectively with interior melt. Similarly to the case at the surface, if the temperature in a layer is above the freezing point, it is set equal to  $T_f$ . To take into account the excess energy that goes into melting, the thickness of ice  $\Delta h_{melt}$  that can be melted by that energy is calculated and incorporated into the surface melt. The thickness  $\Delta h_{melt}$  can be found using the following:

$$c_{p0}(T_f - T)\rho_i dz_i = L_{f0} \left(1 + \frac{\mu_e S}{T}\right) \rho_i \Delta h_{melt}$$

After calculating  $\Delta h_{melt}$  in every layer with melt, the new ice thickness over timestep dt is calculated as:

$$h_i = h_i + \left(\frac{\partial s_i}{\partial t}\right) dt + \sum \Delta h_{melt}$$

The same process is also used in the case of a melting snow cover when many layers are used.

## **B** Model Validation

To test the implementation of the numerical scheme for the biomass and nutrient equations, I ensure that the model conserves B and N, i.e., that the temporal change of B and N is equal to the sources minus the sinks. All tests are run over the study period using data from the PAR site. It is possible to use any forcing data, but this site is used because it is known to include both growing and melting phases. In each test biomass and nutrient concentrations are initially set to zero in all layers except the bottom layer, where they are set to:

$$B(z=1,t=0)=55~{
m mg~chla~m}^{-3}$$
 and  $N(z=1,t=0)=55~{
m mmol~m}^{-3}$ 

Integrating over all 55 ice layers  $(N_{layer})$  and using the initial ice thickness  $h_i$  = 1.6 m, the total initial biomass and nutrients are:

$$B(z = 1, t = 0) * \frac{h_i}{N_{layer}} = 1.6 \text{ mg chla m}^{-2}$$

and

$$N(z = 1, t = 0) * \frac{h_i}{N_{lawer}} = 1.6 \text{ mmol m}^{-2}$$

## B.1 Nutrients and algae advection

I first validate the advection of algae and nutrients through the ice. To this end, the algal growth rate, nutrient uptake rate and nutrient flux are set to zero. In this case, when the ice grows, any difference in biomass and nutrient concentrations in the bottom layer can be accounted for by advection into

higher layers. For simplicity I also set the advection velocity below the bottom layer to zero so that algae and nutrients do not show a gain/loss from intake/expulsion from or into the water. Thus I ensure that the biomass and nutrients present at the end of the model simulation will be equal to the initial values. Thus at each time t:

$$\int_{\hat{z}=b_i}^{s_i} B(z,t) d\hat{z} = \int_{\hat{z}=b_i}^{s_i} B(z,0) d\hat{z} \text{ mg chla m}^{-2}$$

$$\int_{\hat{z}=b_{i}}^{s_{i}} N(z,t)d\hat{z} = \int_{\hat{z}=b_{i}}^{s_{i}} N(z,0)d\hat{z} \text{ mg chla m}^{-2}$$

Figure 18 shows the total biomass and nutrients in the ice during the simulation. In both cases, the total B and N remains constant and equal to the initial value. In the case of the nutrients, advection into higher ice layers is present, while the total biomass remains in the bottom layer. This is due to the advection velocity above the basal layer which does not exceed  $w_{crit} = 1.5$   $cm\ d^{-1}$ . Therefore algae are able to maintain their position (see Figure 18a). When  $w_{crit}$  is set to zero, biomass becomes advected into higher layers in the exact same manner as nutrients (not shown).

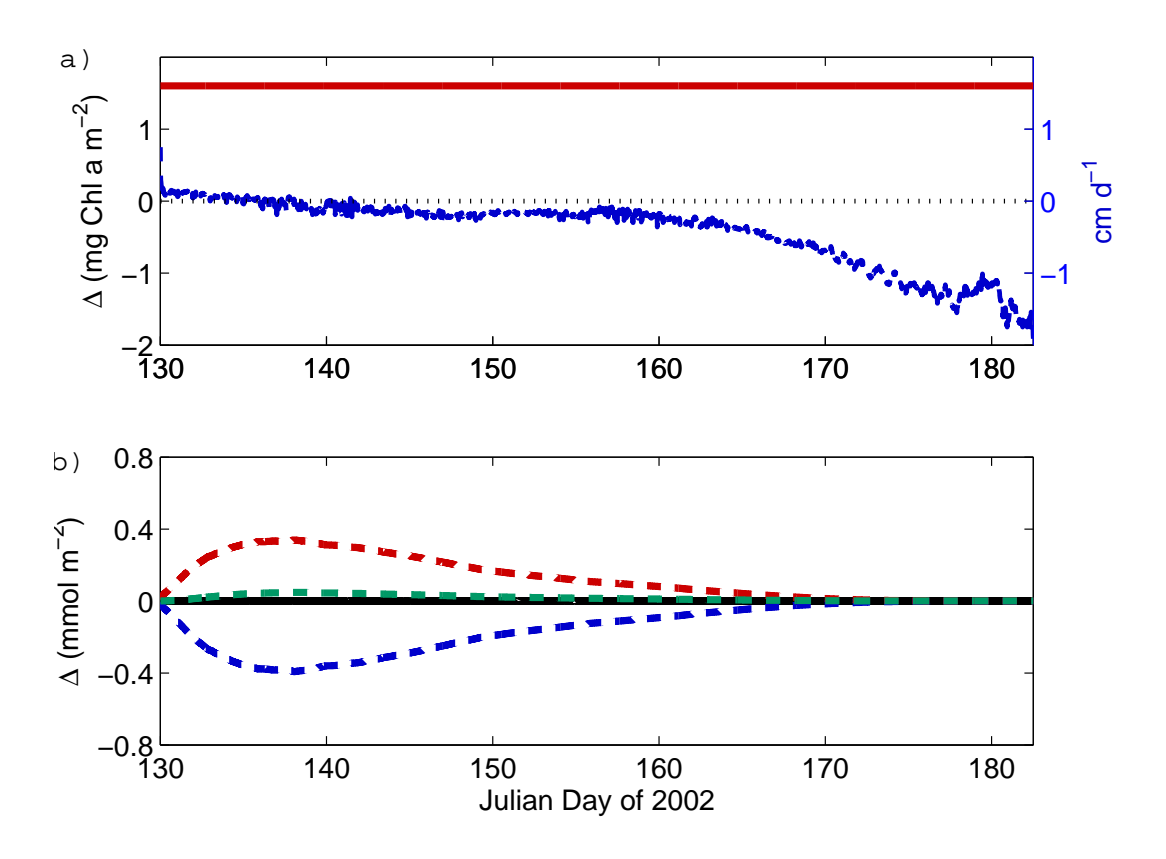


Figure 18: Time series of (a) total biomass in the ice (solid red line), change in total biomass (dotted black line) and the advection velocity at the top of the bottom layer, w(2) (dashed blue line). The concentration in layers 2 and 3 remain equal to zero and are not shown (b) Change in total nutrient concentration (solid black line), and the concentration in the bottom layer (dashed blue line), layer 2 (red dashed line) and layer 3 (green dashed line).

#### B.2 Algae/nutrient loss at ice base

To ensure that the model correctly calculates the amount of algae and nutrients that are expelled into the water column during ice melt, internal sources and sinks of algae/nutrients are again set to zero, but in this case the advection velocity at the ice base is non-zero to allow for loss due to ice melt. In this test, the advective velocity - tested in the previous section - are not reset to zero. Between time t and  $t - \Delta t$  I expect the melt loss of algae  $B_{loss}$  to be equal to:

$$B_{loss}(t) = B(t) - B(t - \Delta t) = w_0 \frac{\Delta t}{\Delta z} B(1, t - \Delta t)$$

and similarly for melt loss of nutrients  $N_{loss}$ 

$$N_{loss}(t) = N(t) - N(t - \Delta t) = w_0 \frac{\Delta t}{\Delta z} N(1, t - \Delta t)$$

where  $B(1, t - \Delta t)$  and  $N(1, t - \Delta t)$  are the biomass and nutrients in the bottom ice layer j = 1 and  $w_0$  is the advection velocity at the ice base. For each  $\Delta t$ , the loss of biomass and nutrients in the bottom ice layer must equal the amount of biomass and nutrients leaving the ice through melting. The sum of nutrients in all ice layers at time t and the nutrients lost through melt must be equal to the initial amount present in the ice:

$$\int_{\hat{z}=b_{i}}^{s_{i}} N(z,t)d\hat{z} + \int_{\hat{t}=0}^{t} N_{loss}d\hat{t} = \int_{\hat{z}=b_{i}}^{s_{i}} N(z,0)d\hat{z}$$

$$\int_{\hat{z}=b_i}^{s_i} B(z,t)d\hat{z} + \int_{\hat{t}=0}^{t} B_{loss}d\hat{t} = \int_{\hat{z}=b_i}^{s_i} B(z,0)d\hat{z}$$

Each term in the above equation are plotted in Figure 19.

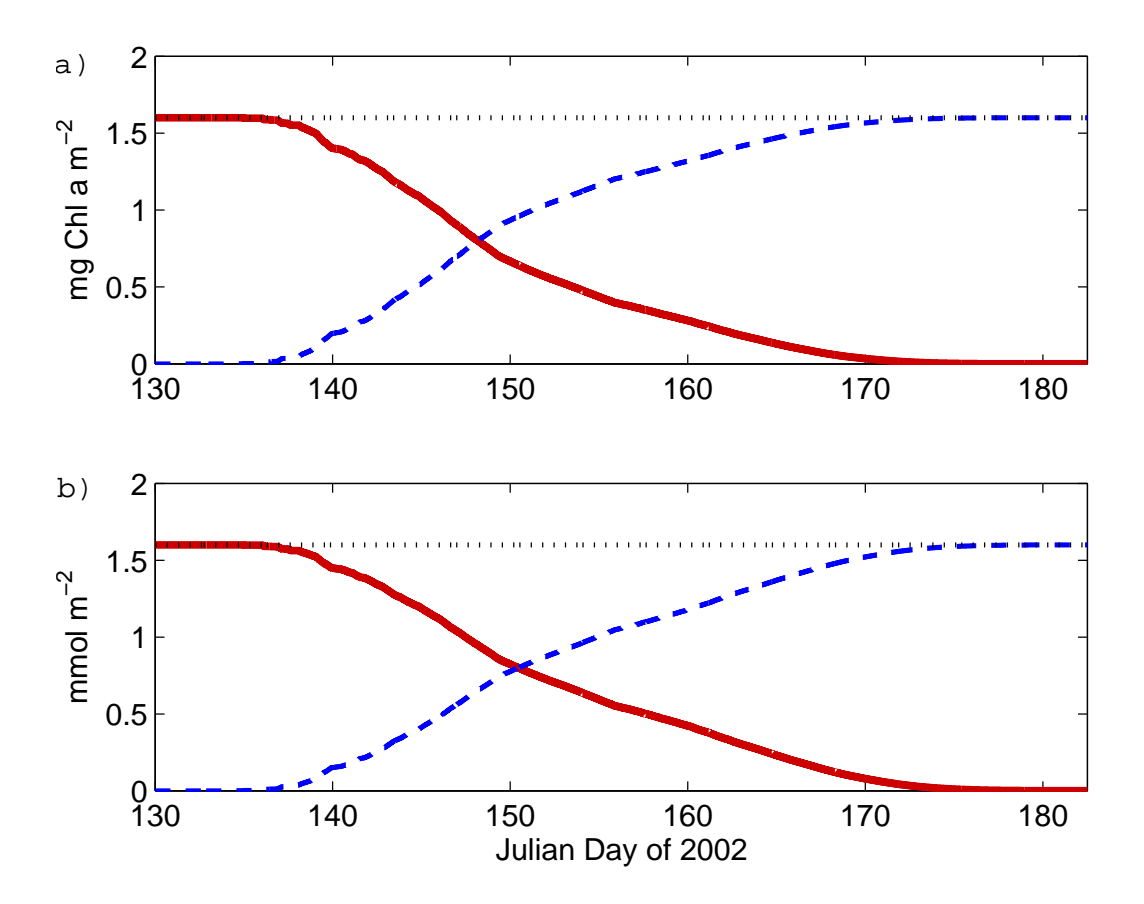


Figure 19: Time series of (a) biomass and (b) nutrients present in the ice (solid red lines), lost at the ice base due to basal melting (dashed blue lines), and the sum of both terms (dotted black lines), equal to B and N total initial concentrations.

#### B.3 Nutrient influx at the ice base

I next test the implementation of the flux of nutrients between the upper water column and the ice base. In this test I keep everything the same as in the previous test, except for the basal flux, which is set is now non-zero. In this case, the sum of nutrients in all layers at time t and the difference between the total input of nutrients from the base between time t and t = 0 and the loss of nutrients due to melt must add up to the initial amount of nutrients, i.e.:

$$\int_{\hat{z}=b_i}^{s_i} N(z,t)d\hat{z} + \int_{\hat{t}=0}^{t} (N_{loss} - F_N)d\hat{t} = \int_{\hat{z}=b_i}^{s_i} N(z,0)d\hat{z}$$

The upper water column data used by the model as input varies with time but values for the nutrient concentration below the ice do not exceed 25 mmol m<sup>-3</sup>. Therefore with the initial nutrient concentration chosen to be 55 mmol m<sup>-3</sup>, I expect the flux of nutrients to be initially negative for this test (from the ice into the water). Both the nutrient flux and nutrients lost through melt are integrated over time and compared with nutrients present in the ice (Figure 20)

#### B.4 Nutrient uptake

Thus far I have shown that the model correctly handles the advection of nutrients and ice algae and the nutrient flux at the ice base. In the following test, the conservation of nutrients and algae is examined with a non-zero uptake of nutrients by algae. Without loss of generality and for simplicity I set the nutrient flux at the ice base  $F_N = 0$ , and set  $L_{lim} = 1$  so that algal growth (in turn influencing the rate of nutrient uptake) is only limited by the nutrient supply. The advection velocities above and below the bottom layer are set to

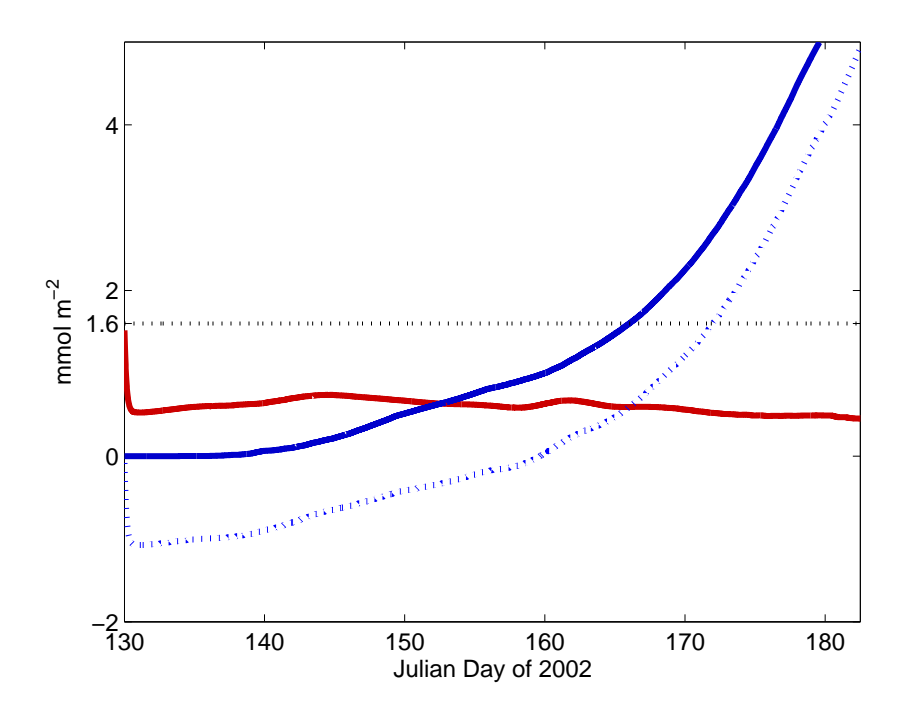


Figure 20: Time series of total nutrients in the ice (solid red line), total nutrient influx at the ice base (dotted blue line), total nutrient lost through melt (solid blue line), and the sum of all 3 terms (black dotted line), equal to the total initial nutrient concentration.

zero to ensure the algae and nutrients are constrained to the bottom layer, again for simplicity. For conservation, the difference in nutrients present in the ice between time t and  $t + \Delta t$  must be equal to the uptake of nutrients by ice algae over a time period  $\Delta t$ , while the difference in algae present in the ice must be equal to the newly grown algae, ie:

$$N(1, t + \Delta t) - N(1, t) = -\int_{\hat{t}=t}^{t+\Delta t} N_{up}(1, t) d\hat{t}$$
 (24)

$$B(1, t + \Delta t) - B(1, t) = \int_{\hat{t}=t}^{t+\Delta t} \mu B(1, t) d\hat{t}$$
 (25)

Since light is not a limiting factor in this test, the growth rate  $\mu$  depends only on the maximum growth rate  $\mu_{max}$  and the nutrient limitation  $N_{lim}$ . The left-hand sides (LHS) and right-hand sides (RHS) of the above equations are plotted in Figure 21. Recalling the definitions of  $N_{up}$ ,  $\mu$  and  $N_{lim}$  (see equations 7 - 10), they can be written as:

$$-\int_{\hat{t}=t}^{t+\Delta t} N_{up}(1,t)d\hat{t} = -\int_{\hat{t}=t}^{t+\Delta t} \mu B \frac{N}{Chla} d\hat{t},$$

$$= -\int_{\hat{t}=t}^{t+\Delta t} \mu_{max} N_{lim} B \frac{N}{Chla} d\hat{t},$$

$$\int_{\hat{t}=t}^{t+\Delta t} \mu B(1,t) d\hat{t} = \int_{\hat{t}=t}^{t+\Delta t} \mu_{max} N_{lim} B d\hat{t}.$$

In addition to the LHS and RHS of equations (24) and (25), Figure 21 also compares total simulated B and N in the ice to B and N calculated using the RHS. Results are shown only over the first 3 days of the model run (Figure 21) because algae and nutrient levels plateau within that period. A small discrepancy between simulated and calculated B on the third day, because the calculations were done explicitly rather than implicitly as in the model.

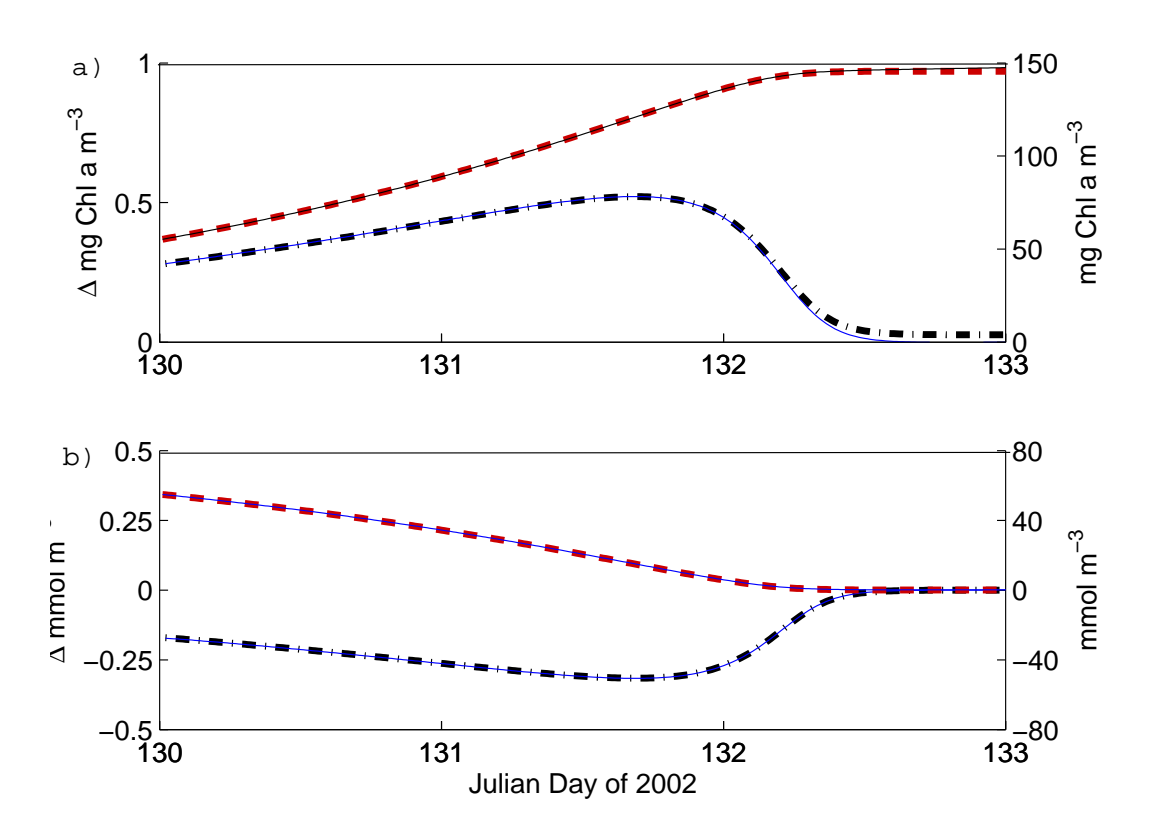


Figure 21: Time series of a) biomass and b) nutrients calculated (black lines) and simulated (dashed lines) of totals (red lines, right axes) and changes per timestep (blue lines, left axes).

In the case with no nutrient flux from the ocean mixed layer, non-zero algae and no light limitation, I expect that nutrients would decay exponentially until reaching zero (see equations 5 - 10). Similarly I expect algae to grow exponentially until nutrients run out. The level at which the algae plateaus is something that the model must correctly predict. The governing equations for ice algae and nutrients (see equations 5 and 6) are non-linear, making them difficult to solve. However a simple way to find an answer is to first notice the similarity of the governing equations when  $F_N$  and  $L_{lim}$  are omitted. Again using equations 7, 8 and 10, and substituting into equation 6, I have:

$$\frac{\partial N}{\partial t} = -N_{up}$$

$$= -\mu B \frac{N}{Chla}$$

$$= -\mu_{max} N_{lim} B \frac{N}{Chla}$$

$$= -\mu_{max} \frac{N}{K_s + N} B \frac{N}{Chla}$$
and
$$\frac{\partial B}{\partial t} = \mu B$$

$$= \mu_{max} \frac{N}{K_s + N} B$$

Since N/Chla is taken as a constant in this study, there is a simple relation between the rate of change of B and N, namely:

$$\frac{\partial B}{\partial t} = -\frac{1}{N/Chla} \frac{\partial N}{\partial t}$$

With initial values of N(1,0) = 55 mmol m<sup>-3</sup> and B(1,0) = 55 mg chla m<sup>-3</sup>, the algae level B(1,T) at time T when nutrients become zero will be equal to:

$$\frac{B(1,T) - B(1,0)}{\Delta t} = -\frac{1}{N/Chla} \frac{N(1,T) - N(1,0)}{\Delta t}$$

$$B(1,T) = B(1,0) - \frac{N(1,T) - N(1,0)}{N/Chla}$$
$$= 55 - \frac{0 - 55}{N/Chla}$$
$$\doteq 146$$

Thus biomass should plateau at around 146 mg chla m<sup>-3</sup>, in agreement with results shown in Figure 21. Because the model output shows an exponential growth of algae before nutrient limitation occurs (as expected from the simplified governing equation), and also reaches the predicted plateau level of maximum biomass for nutrients available, I am confident that the model is correctly calculating the algal growth based on the equations.